New distances to RAVE stars

J. Binney,[1]* B. Burnett,[1] G. Kordopatis,[2] P. J. McMillan,[1] S. Sharma,[3] T. Zwitter,[4,5]
O. Bienaymé,[6] J. Bland-Hawthorn,[3] M. Steinmetz,[7] G. Gilmore,[2] M. E. K. Williams,[7]
J. Navarro,[8] E. K. Grebel,[9] A. Helmi,[10] Q. Parker,[11] W. A. Reid,[11] G. Seabroke,[12]
F. Watson[13] and R. F. G. Wyse[14]

[1]*Rudolf Peierls Centre for Theoretical Physics, Keble Road, Oxford OX1 3NP, UK*
[2]*Institute of Astronomy, Madingley Road, Cambridge CB3 0HA, UK*
[3]*Sydney Institute for Astronomy, University of Sydney, School of Physics A28, NSW 2006, Australia*
[4]*Faculty of Mathematics and Physics, University of Ljubljana, Jadranska 19, 1000 Ljubljana, Slovenia*
[5]*Slovenia and Center of Excellence SPACE-SI, Aškerčeva cesta 12, 1000 Ljubljana, Slovenia*
[6]*Observatoire Astronomique de Strasbourg, 11 rue de l'Université, F-67000 Strasbourg, France*
[7]*Leibniz-Institut für Astrophysik Potsdam (AIP), An der Sternwarte 16, D-14482 Potsdam, Germany*
[8]*Department of Physics & Astronomy, University of Victoria, 3800 Finnerty Rd, Victoria, V8P 5C2, Canada*
[9]*Astronomisches Rechen-Institut, Zentrum für Astronomie der Universität Heidelberg, Mönchhofstr 12-14, D-69120 Heidelberg, Germany*
[10]*Kapteyn Astronomical Institut, University of Groningen, Landleven 12, NL-9747 AD Groningen, the Netherlands*
[11]*Macquarie University, Sydney, Australia*
[12]*Mullard Space Science Laboratory, University College London, Holmbury St Mary, Dorking RH5 6NT, UK*
[13]*Australian Astronomical Observatory, PO Box 296, Epping, NSW 1710, Australia*
[14]*Department of Physics and Astronomy, Johns Hopkins University, 366 Bloomberg centre, 3400 N. Charles St., Baltimore, MD 21218, USA*

ABSTRACT

Probability density functions (pdfs) are determined from new stellar parameters for the distance moduli of stars for which the RAdial Velocity Experiment (RAVE) has obtained spectra with $S/N \geq 10$. Single-Gaussian fits to the pdf in distance modulus suffice for roughly half the stars, with most of the other half having satisfactory two-Gaussian representations. As expected, early-type stars rarely require more than one Gaussian. The expectation value of distance is larger than the distance implied by the expectation of distance modulus; the latter is itself larger than the distance implied by the expectation value of the parallax. Our parallaxes of *Hipparcos* stars agree well with the values measured by *Hipparcos*, so the expectation of parallax is the most reliable distance indicator. The latter are improved by taking extinction into account. The effective temperature–absolute magnitude diagram of our stars is significantly improved when these pdfs are used to make the diagram. We use the method of kinematic corrections devised by Schönrich, Binney and Asplund to check for systematic errors for general stars and confirm that the most reliable distance indicator is the expectation of parallax. For cool dwarfs and low-gravity giants, $\langle \varpi \rangle$ tends to be larger than the true distance by up to 30 per cent. The most satisfactory distances are for dwarfs hotter than 5500 K. We compare our distances to stars in 13 open clusters with cluster distances from the literature and find excellent agreement for the dwarfs and indications that we are overestimating distances to giants, especially in young clusters.

Key words: stars: distances – dust extinction – solar neighbourhood – stellar content – structure.

1 INTRODUCTION

Surveys of the stellar content of our Galaxy are key to the elucidation of the Galaxy's structure and history. Consequently, over

the last decade considerable observational resources have been devoted to such surveys. Three surveys are particularly worthy of note: the 2MASS (Strutskie et al. 2006), the Sloan Digital Sky Survey (SDSS; York et al. 2000; Yanny et al. 2009) and the RAdial Velocity Experiment (RAVE; Steinmetz et al. 2006; Siebert et al. 2011). The 2MASS was an all-sky, near-infrared photometric survey, while the SDSS combined a photometric survey in the *ugriz*

system with spectroscopy for a subset of objects with spectral resolution $R = 2500$. The RAVE survey has taken spectra at resolution $R \simeq 7500$ of $\sim$500 000 stars that have 2MASS photometry. The RAVE and SDSS surveys are complementary in that SDSS worked at apparent magnitudes $r \gtrsim 18$ so faint that it catalogued mainly dwarf stars that lie more than 500 pc from the Sun, while RAVE operates at apparent magnitudes $I \approx 9$–13 and observes both nearby dwarfs and giants at distances up to $\sim$4 kpc (Burnett et al. 2011).

Although the ideal way to extract science from a survey is to project models into the space of observables, i.e. sky coordinates, line-of-sight velocity, apparent magnitudes, etc., and fit the projected models to the data (e.g. Binney 2011); in practice one generally assigns a distance to each star and uses this distance to place the star in the space in which physics applies, namely phase space complemented with luminosity, colour, chemical composition, etc. Since RAVE's targets overwhelmingly lie beyond the range of *Hipparcos* and include both dwarfs and giants, the task of assigning distances to these stars is complex. To date three papers (Breddels et al. 2010; Zwitter et al. 2010; Burnett et al. 2011) address this task with techniques of increasing sophistication. Results presented in those papers are based on stellar parameters produced by the pipeline that was developed for analysis of the RAVE spectra. This pipeline was described in the papers that accompanied the second and third releases of RAVE data (Zwitter et al. 2008; Siebert et al. 2011). Between those two data releases changes were made to the pipeline's parameters that were designed to improve the accuracy of the derived metallicities, but the parameters from neither version of the pipeline were entirely satisfactory (Burnett et al. 2011, hereafter B11).

On account of residual internal and external inconsistencies in the parameters, a completely new pipeline has been developed for the analysis of RAVE spectra. This pipeline and the stellar parameters it produces are described in Kordopatis et al. (2013). The new stellar parameters form a much more compelling and consistent data base than the old ones, and their arrival prompts us to revisit the assignment of distances using the new parameters as inputs.

We use the Bayesian framework described by Burnett & Binney (2010) but modified to allow for the impact of interstellar dust. Two other significant novelties are (i) the production of multi-Gaussian fits to each star's probability density function (pdf) in distance modulus and (ii) the use of the kinematic correction factors introduced by Schönrich, Binney & Asplund (2012a) to check for systematic errors in our distances. We have derived distances for all stars that have spectra to which the new pipeline assigns a signal-to-noise ratio (S/N) of 10 or higher. These distances are contained in RAVE's fourth data release, and the RAVE collaboration recommends the use of these distances. When a star has more than one spectrum in the data base, the catalogued distance is that derived from the highest S/N spectrum.

The plan of the paper is as follows. In Section 2, we recapitulate the principles of Bayesian distance determination and describe how we take extinction into account. In Section 3, we discuss typical pdfs in distance modulus and explain how we produce multi-Gaussian fits to them. In Section 4, we compare our spectrophotometric parallaxes to *Hipparcos* parallaxes and describe how these comparisons are affected by neglecting extinction. In Section 5, we analyse our distances to the generality of stars, using kinematic correction factors to test for systematic biases in distances as functions of surface gravity or effective temperature, and to modify distance pdfs (Section 5.1). In Section 6, we compare our distances to cluster stars with the established distances to their clusters. In Section 7, we examine the scatter in the distances to the same star obtained from different

spectra. In Section 8, we examine the distribution of extinctions to stars. Section 9 sums up.

2 METHODOLOGY

As in B11 we start from the trivial Bayesian statement

$$p(\text{model}|\text{data}) = \frac{p(\text{data}|\text{model}) \, p(\text{model})}{p(\text{data})}, \tag{1}$$

where 'data' comprises the observed parameters and photometry of an individual star and 'model' comprises a star of specified initial mass $\mathcal{M}$, age τ, metallicity [*M/H*] and location. We use $p(\text{model}|\text{data})$ either to calculate expectation values $\langle x \rangle$ and dispersions σ_x of quantities of interest, such as the stars's distance $x = s$ and parallax $x = \varpi$, by integrating $P(\text{model}|\text{data})$ times an appropriate power of x through the space spanned by the model parameters [*M/H*], τ, $\mathcal{M}$, ..., or the pdf in distance modulus by marginalizing $P(\text{model}|\text{data})$ over all model parameters other than distance.

A key role is played by the prior probability $p(\text{model})$, which reflects our prior knowledge of the Galaxy: massive young stars are rarely found far from the plane, while a star far from the plane is likely to be old and have subsolar abundances. We have used the same three-component prior used in B11:

$$p(\text{model}) = p(\mathcal{M}) \sum_{i=1}^{3} p_i([M/H]) \, p_i(\tau) \, p_i(\mathbf{r}), \tag{2}$$

where $i = 1, 2, 3$ correspond to a thin disc, thick disc and stellar halo, respectively. We assumed an identical Kroupa-type initial mass function (IMF) for all three components and distinguish them as follows:

Thin disc ($i = 1$):

$$p_1([M/H]) = G([M/H], 0.2),$$

$$p_1(\tau) \propto \exp(0.119 \, \tau/\text{Gyr}) \quad \text{for } \tau \leq 10 \, \text{Gyr},$$

$$p_1(\mathbf{r}) \propto \exp\left(-\frac{R}{R_d^{\text{thin}}} - \frac{|z|}{z_d^{\text{thin}}}\right); \tag{3}$$

Thick disc ($i = 2$):

$$p_2([M/H]) = G([M/H] + 0.6, 0.5),$$

$$p_2(\tau) \propto \text{uniform in range } 8 \leq \tau \leq 12 \, \text{Gyr},$$

$$p_2(\mathbf{r}) \propto \exp\left(-\frac{R}{R_d^{\text{thick}}} - \frac{|z|}{z_d^{\text{thick}}}\right); \tag{4}$$

Halo ($i = 3$):

$$p_3([M/H]) = G([M/H] + 1.6, 0.5),$$

$$p_3(\tau) \propto \text{uniform in range } 10 \leq \tau \leq 13.7 \, \text{Gyr},$$

$$p_3(\mathbf{r}) \propto r^{-3.39}, \tag{5}$$

where R signifies the Galactocentric cylindrical radius, z cylindrical height and r spherical radius, and $G(x, y)$ is a Gaussian distribution in x of zero mean and dispersion y. The parameter values were taken as in Table 1; the values are taken from the analysis of SDSS data in Jurić et al. (2008). The metallicity and age distributions for the thin disc come from Haywood (2001) and Aumer & Binney (2009), while the radial density of the halo comes from the 'inner halo' detected in Carollo et al. (2009). The metallicity and age distributions of the thick disc and halo are influenced by Reddy (2009) and Carollo et al. (2009).

Table 1. Values of disc parameters used.

Parameter	Value (pc)
R_d^{thin}	2600
z_d^{thin}	300
R_d^{thick}	3600
z_d^{thick}	900

Table 2. Metallicities of isochrones used, taking $(Z_\odot, Y_\odot) = (0.017, 0.260)$.

Z	Y	$[M/H]$
0.0022	0.230	−0.914
0.003	0.231	−0.778
0.004	0.233	−0.652
0.006	0.238	−0.472
0.008	0.242	−0.343
0.010	0.246	−0.243
0.012	0.250	−0.160
0.014	0.254	−0.090
0.017	0.260	0.000
0.020	0.267	0.077
0.026	0.280	0.202
0.036	0.301	0.363
0.040	0.309	0.417
0.045	0.320	0.479
0.050	0.330	0.535
0.070	0.372	0.727

The normalizations were then adjusted so that at the solar position, taken as $R_0 = 8.33$ kpc (Gillessen et al. 2009), $z_0 = 15$ pc (Binney, Gerhard & Spergel 1997; Jurić et al. 2008), we have number density ratios $n_2/n_1 = 0.15$ (Jurić et al. 2008) and $n_3/n_1 = 0.005$ (Carollo et al. 2009).

The IMF chosen follows the form originally proposed by Kroupa, Tout & Gilmore (1993), with a minor modification following Aumer & Binney (2009), being

$$p(\mathcal{M}) \propto \begin{cases} \mathcal{M}^{-1.3} & \text{if } \mathcal{M} < 0.5\,\text{M}_\odot, \\ 0.536\,\mathcal{M}^{-2.2} & \text{if } 0.5 \leq \mathcal{M} < 1\,\text{M}_\odot, \\ 0.536\,\mathcal{M}^{-2.519} & \text{otherwise.} \end{cases} \quad (6)$$

We predicted the photometry of stars from the isochrones of the Padova group (Bertelli et al. 2008), which provide tabulated values for the observables of stars with metallicities ranging upwards from around $[M/H] \approx -0.92$, ages in the range $\tau \in [0.01, 19]$ Gyr and masses in the range $\mathcal{M} \in [0.15, 20]$ M$_\odot$. We used isochrones for 16 metallicities as shown in Table 2, selecting the helium mass fraction Y as a function of the metal mass fraction Z according to the relation used in Aumer & Binney (2009), i.e. $Y \approx 0.225 + 2.1Z$ and assuming solar values of $(Y_\odot, Z_\odot) = (0.260, 0.017)$. The metallicity values were selected by eye to ensure that there was not a great change in the stellar observables between adjacent isochrone sets.

In B11 no correction was made for the differences between the Johnson–Cousins–Glass photometric system used for the Padova stellar models that we use and the 2MASS system. Here we use the transformations of Koen et al. (2007) to transform the 2MASS magnitudes $J_2, \ldots$ to the Johnston–Cousins–Glass magnitudes

$J, \ldots$:

$$J = 0.029 + J_2 + 0.07(J_2 - K_2) - 0.045(J_2 - H_2)^2$$

$$H = H_2 + 0.555(H_2 - K_2)^2 - 0.441(H_2 - K_2) + 0.089(J_2 - H_2)$$

$$K = 0.009 + K_2 + 0.195(J_2 - H_2)^2 - 0.156(J_2 - H_2)$$

$$+ 0.304(H_2 - K_2) - 0.615(H_2 - K_2)^2. \quad (7)$$

Unless explicitly stated to the contrary, we will state *JHK* magnitudes in the Johnston–Cousins–Glass system.

Dust both dims and reddens stars. Let the column of dust between us and a given star produce optical extinction A_V, then from Rieke & Lebofsky (1985) we take the extinctions to be

$$A_J = 0.282 A_V$$

$$A_H = 0.175 A_V$$

$$A_K = 0.112 A_V. \quad (8)$$

In B11 A_V was set identically to zero and the H magnitude was not employed. Here we include the H magnitude in the set of observations so we have three constraints on the star's spectral distribution: the spectroscopically derived T_{eff} and two IR colours. Consequently, we should be able to constrain the extinction to some extent. We integrate over all possible values of A_V. We include A_V in the prior by multiplying the prior (2) by the probability density of A_V. Since A_V is an intrinsically non-negative quantity, a completely flat prior would be one uniform in $a \equiv \ln(A_V)$. We do not want a flat prior but one that reflects increasing extinction with distance and higher extinction towards the Galactic Centre than towards the poles. Let $a_{\text{prior}}(\boldsymbol{x})$ be the expected value of $\ln(A_V)$ for the location $\boldsymbol{x}$. Then a natural choice for the probability of extinctions associated with the interval $(a, a + da)$ is

$$dP = (2\pi\sigma^2)^{-1/2} e^{-(a - a_{\text{prior}})^2 / 2\sigma^2} da$$

$$= (2\pi\sigma^2)^{-1/2} e^{-\ln^2(A_V / A_{V\text{prior}}) / 2\sigma^2} da. \quad (9)$$

The dispersion σ reflects the random fluctuation of the extinction from one sight line to the next on account of the cloudy nature of the interstellar medium (ISM). We have rather arbitrarily set $2\sigma^2 = 1$.

$A_{V\text{prior}}$ is related to distance by

$$A_{V\text{prior}}(b, \ell, s) = A_{V\infty}(b, \ell) \frac{\int_0^s ds' \, \rho[\boldsymbol{x}(s')]}{\int_0^\infty ds' \, \rho[\boldsymbol{x}(s')]}, \quad (10)$$

where $\boldsymbol{x}(s)$ is the position vector of the point that lies distance s down the line of sight (b, ℓ), $A_{V\infty}(b, \ell)$ is defined below and $\rho(\boldsymbol{x})$ is a model of the density of extincting material. Following Sharma et al. (2011), we adopt

$$\rho(\boldsymbol{x}) = \exp\left[\frac{R_0 - R}{h_R} - \frac{|z - z_{\text{w}}|}{k_{\text{fl}} h_z}\right], \quad (11)$$

where $k_{\text{w}}(R)$ and $z_{\text{w}}(R)$ describe the flaring and warping of the gas disc:

$$k_{\text{fl}}(R) = 1 + \gamma_{\text{fl}} \min(R_{\text{fl}}, R - R_{\text{fl}})$$

$$z_{\text{w}}(R, \phi) = \gamma_{\text{w}} \min(R_{\text{w}}, R - R_{\text{w}}) \sin\phi. \quad (12)$$

Here ϕ is the Galactocentric azimuth that increases in the direction of Galactic rotation and places the Sun at $\phi = 0$. Table 3 gives the values of the parameters that occur in these formulae.

We take the extinction to infinity, $A_{V\infty}(b, \ell)$, from observation: except along exceptionally obscured lines of sight, $A_{V\infty}$ is 3.1 times

Table 3. Parameters of the model of the dust distribution. Distances are in kiloparsecs.

$A_V(0)$	h_R	h_z	R_{fl}	γ_{fl}	R_w	γ_w
1.67	4.2	0.088	$1.12R_0$	0.0054	8.4	0.18

the reddening estimated by Schlegel, Finkbeiner & Davis (1998). However, Arce & Goodman (1999) pointed out that Schlegel et al. overestimate the reddening in regions with $E(B - V) > 0.15$. Following Sharma et al. (2011), we correct for this effect by multiplying the Schlegel et al. values of $E(B - V)$ by the correction factor

$$f(E(B - V)) = 0.6 + 0.2 \left[1 - \tanh \left(\frac{E(B - V) - 0.15}{0.3} \right) \right],$$
(13)

which has the effect of leaving $E(B - V)$ invariant for $E(B - V) \lesssim 0.16$ and multiplying large values of $E(B - V)$ by a factor 0.6.

The function $A_{V\text{prior}}(s)$ is tabulated on a non-uniform grid in s before each star is analysed so $A_{V\text{prior}}$ can be subsequently obtained quickly by linear interpolation.

Given a model star characterized by ([M/H],τ, $\mathcal{M}$), a first estimate of the distance to the star is made under the assumption $A_V = 0$. Then $A_{V\text{prior}}$ is evaluated for this distance and a second estimate of distance obtained, and $A_{V\text{prior}}$ is evaluated at this improved distance and stored as $A_{V\text{model}}$. The reddened $J - K$ colour of the star is now predicted and compared with the observed colour. The given model star is considered sufficiently plausible to be worth considering further only if both its colour reddened by e times $A_{V\text{model}}$ is redder than the blue end of the 3σ range around the measured colour and the star's colour reddened by 1/e times $A_{V\text{model}}$ is bluer than the red end of the measured 3σ range. If these conditions are satisfied, we consider values of A_V that lie the range $(e^{-1.5}, e^{1.5})A_{V\text{model}}$. For each value of A_V, all plausible distances are considered.

We calculate the expectation $\langle a \rangle$ of $a \equiv \ln A_V$ and use $\widetilde{A}_V \equiv \exp(\langle a \rangle)$ as our final estimate of the extinction to each star.

3 PDFS FOR DISTANCE

The Bayesian argument yields the five-dimensional pdf that each star has a given mass, metallicity, age, line-of-sight extinction and distance, but Burnett & Binney (2010) and B11 reported only the im-

plied means and standard deviations of distance and parallax. Hence, they had two logically independent measures of the distance to a star: $\langle s \rangle$ and $1/\langle \varpi \rangle$. A third natural distance measure is provided by the expectation of the distance modulus $\mu = 5\log_{10}(s/10\,\text{pc})$. We shall show that these three measures yield systematically different distances and conclude that $1/\langle \varpi \rangle$ is the most reliable estimate.

A logical next step is to inspect the pdfs we obtain for s, etc., after marginalizing over the star's other properties. If any of these pdfs is well approximated by a Gaussian, it can be fully characterized by its mean and dispersion. In this section, we show that the pdfs often deviate significantly from a Gaussian, and in this case it is important to know more than the pdf's mean and dispersion.

Fig. 1 shows pdfs in distance modulus for three stars. The red curves show Gaussian distributions in distance modulus $\mu \equiv m - M$, while the green curves show distributions that are Gaussian in distance s and the blue curves show distributions that are Gaussian in parallax ϖ. Given how strongly these three curves differ from one another, especially in the left-hand and centre panels, it is clear that a very particular assumption is being made if one supposes that a star's distribution of either μ, s or ϖ is Gaussian, and if one of these distributions *is* Gaussian, the other two cannot be.

In each panel of Fig. 1, the black curve shows the computed marginalized pdf in distance modulus μ, while the red curve shows Gaussian with the same mean and standard deviation as the computed pdf. The green curve shows the pdf which is a Gaussian in distance and has the mean and standard deviation of the computed pdf in distance, while the blue curve shows the pdf which is a Gaussian in parallax and has the mean and dispersion of the computed pdf in parallax. None of the coloured curves can be considered a reasonable representation of the computed pdf. The clear message of Fig. 1 is that it is dangerous to quantify the distance to these stars in the form $x \pm y$ kpc because this notation implies that a Gaussian pdf adequately approximates the true pdf.

We have derived multi-Gaussian approximations to the pdf in μ since this variable is physically meaningful for any real number. We write

$$P(\mu) = \sum_{k=1}^{N} \frac{f_k}{\sqrt{2\pi\sigma_k^2}} \exp \left(- \frac{(\mu - \mu_k)^2}{2\sigma_k^2} \right),$$
(14)

where N, the means μ_k, weights f_k and dispersions σ_i are to be determined. We take bins in distance modulus of width $w_i = 0.2$,
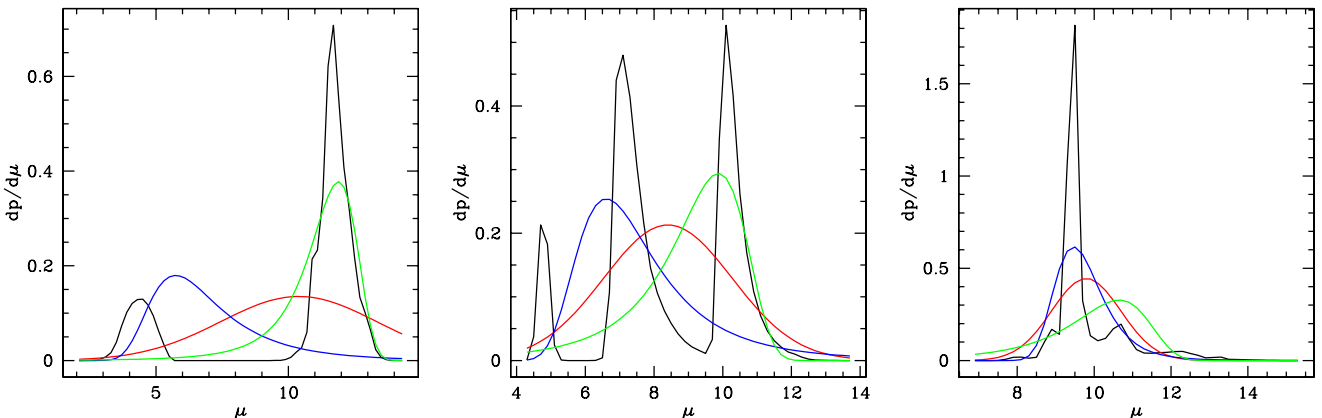

Figure 1. Pdfs in distance modulus for three RAVE stars that are not among the ∼45 per cent of stars with pdfs that can be adequately fitted by a single Gaussian. The black line shows the computed pdf while the red curve shows a Gaussian with the same mean and standard deviation. The blue curve shows the pdf implied by a Gaussian in parallax and the green curve that implied by a Gaussian in distance. Approximately 20 per cent of the pdfs are bimodal (left), 5 per cent are trimodal (centre) and 25 per cent are dominated by a sharp peak that sits on a broader component that has a much lower probability *density*, but contributes a significant fraction of the total probability (right).

containing a fraction p_i of the total probability taken from the computed pdf, and a fraction P_i of the total probability taken from the multi-Gaussian approximation and consider the statistic

$$F = \sum_i \left(\frac{p_i}{w_i} - \frac{P_i}{w_i} \right)^2 \tilde{\sigma} w_i, \qquad (15)$$

where the weighted dispersion

$$\tilde{\sigma}^2 \equiv \sum_{k=1,N} f_k \sigma_k^2 \qquad (16)$$

is a measure of the overall width of the pdf. Our definition of F includes the factor $\tilde{\sigma}$ to ensure that F is unchanged when the width of both the true pdf and our approximation is increased by the same factor: this condition ensures that F is a measure of how well the shape of the distribution is fitted. We use $\tilde{\sigma}$ in equation (15) rather than the dispersion of the pdf because in some circumstances (double- or triple-peaked distributions) the dispersion is dominated by the distance between peaks, rather than the widths of the individual peaks themselves, and it is the peaks that should set the scale. A practical difficulty is that F is minimized by letting every $\sigma_k \to 0$. Hence, instead of minimizing F, we minimize the alternative statistic

$$F' = \sum_i \left(\frac{p_i}{w_i} - \frac{P_i}{w_i} \right)^2 w_i \qquad (17)$$

and only use F to measure whether the fit is a sufficiently accurate description of the data.

If the value of F for a Gaussian with the same mean and dispersion in μ as that taken from the computed pdf is less than a threshold value $F_t = 0.04$, we accept this as an adequate description of the data. This condition holds for around 45 per cent of the RAVE stars. When it fails, we use the Levenberg–Marquardt algorithm to minimize F' with $N = 2$ and several different initial choices for the parameters. We accept this description of the data if it gives $F < F_t$ *and* the dispersion of the model is within 20 per cent of that of the complete pdf. The latter condition ensures that we do not accept models that provide an excellent fit to a significant component of the probability but ignore a small but non-negligible component at a different distance. If the two-Gaussian description fails, we fit a three-Gaussian approximation. We reach this stage for around 5 per cent of the RAVE stars because the double-Gaussian approximation is accepted in ∼50 per cent of cases. Fig. 2 shows the multi-Gaussian models fitted to the pdfs shown in Fig. 1.

Any fits for which the dispersion of the fitted model differs by more than 20 per cent from that of the data are flagged as possibly

inadequate. Approximately 4 per cent of the models are flagged for this reason. In Fig. 3, we show some typical examples of the flagged models. We see that the problems are in fact minor ones.

4 *Hipparcos* STARS

As in B11, the primary test of the validity of our spectrophotometric distances is provided by *Hipparcos* stars that are likely to be single stars because in the van Leeuwen (2007) catalogue they have `soln` < 10. There are 5614 distinct stars of this type for which we have RAVE parameters, and the mean S/N of their spectra is 84.

The quoted errors on the stellar parameters play a big role in the Bayesian algorithm, and good results are obtainable only with accurate error estimates. When the data were first processed using only the internal error estimates produced by the spectral-reduction pipeline, manifestly inconsistent results for *Hipparcos* stars were produced. The results were dramatically improved by adding to the internal errors the external errors for various classes of star derived by Kordopatis et al. (2013) and listed in Table 4. The quadrature sums of the internal and external errors prove to be quite similar to the errors adopted by B11, which could not be founded on star-specific error estimates from the old pipeline.

The black points in Fig. 4 show histograms of the discrepancies between *Hipparcos* parallaxes ϖ_H and expectation values of parallaxes obtained from $P(\text{model}|\text{data})$ for three groups of stars: giants ($\log g < 3.5$), hot dwarfs ($T_{\text{eff}} > 5500\,\text{K}$) and cool dwarfs. The parallax differences are normalized by the quadrature sum of the formal errors in the *Hipparcos* data and our adopted errors, so if our procedure were sound and the central limit theorem applied to the data, the histograms would be Gaussians of unit dispersion. This expectation is met to a pleasing extent for hot dwarfs and giants – for the hot dwarfs the mean of the distribution is 0.143 and the dispersion is 1.061 and for the giants they are -0.057 and 1.077. Thus, on average the parallaxes of the hot dwarfs are slightly too large, while those of the giants are slightly too small and our error estimates are only a shade too small. The results for the smaller number of cool dwarfs are less clear-cut: the mean and dispersion are 0.123 and 1.314 implying that our parallaxes are slightly too large and our errors are materially too small.

It is interesting to compute means of the distances ratios. Let

$$xr_{s\mu} \equiv \overline{\langle s \rangle / s_{\langle \mu \rangle}} \quad r_{\mu\varpi} \equiv \overline{s_{\langle \mu \rangle} \langle \varpi \rangle}$$

$$r_{\varpi H} \equiv \overline{\varpi_H / \langle \varpi \rangle} \quad r_{sH} \equiv \overline{\langle s \rangle \varpi_H}, \qquad (18)$$

where overbars imply averages of a group of stars and $s_{\langle \mu \rangle}$ is the distance implied by the expectation value of the distance modulus.
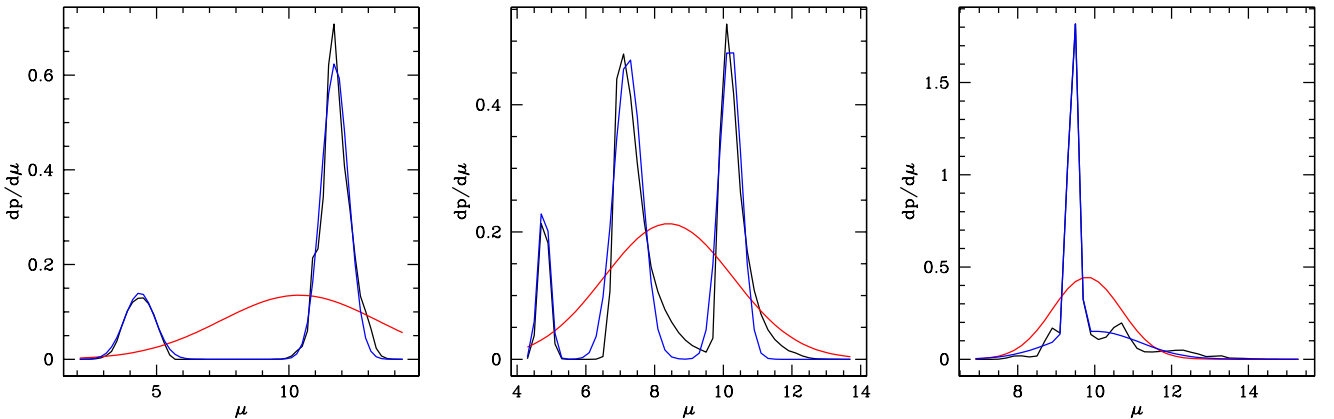

Figure 2. The black curves show the pdfs in distance modulus for the same three stars as in Fig. 1, while the blue line shows the chosen multi-Gaussian fitting.
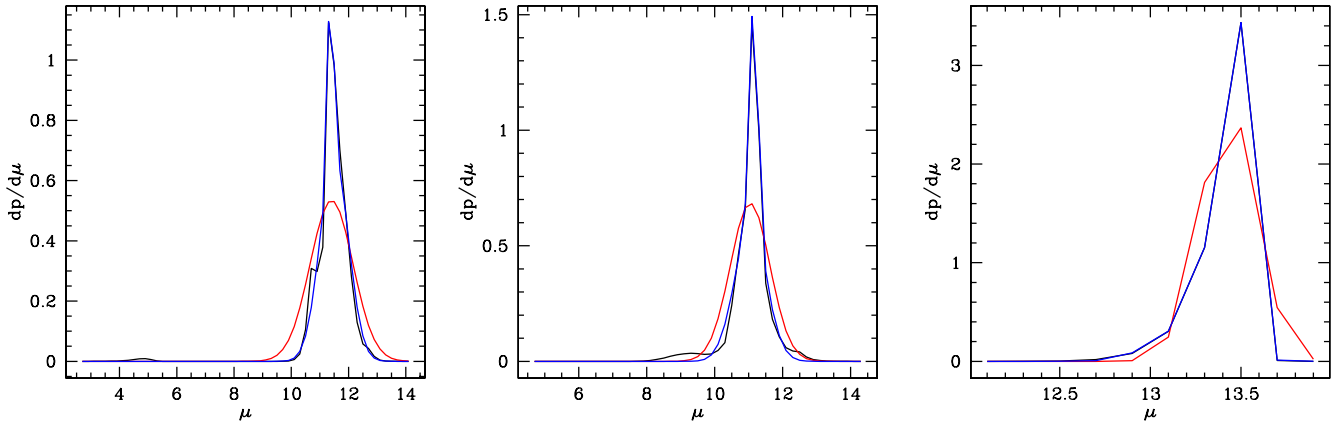
Figure 3. Pdfs in distance modulus for three stars that are flagged as having potentially inadequate multi-Gaussian fits to their pdfs because the true dispersions in μ differ by more than 20 per cent from the dispersions of the fitted models. As in Fig. 2, the black line shows the computed pdf and the blue line shows the output from the multi-Gaussian fitting. The red line shows a Gaussian with the same mean and dispersion. The reason for the flag in the left-hand panel is the very small component of the computed pdf at $\mu \sim 5$, which is not picked up by the fitted pdf. In the centre panel, the flag is raised because the fitted pdf does not fully reflect the broad wings of the pdf. In the right-hand panel, the fit appears nearly perfect, but this reflects the resolution of the histogram (used both to find the approximation and to plot this figure) being low compared to the width of the pdf – the dispersion in distance modulus is 0.15, which is smaller than the histogram bin size.
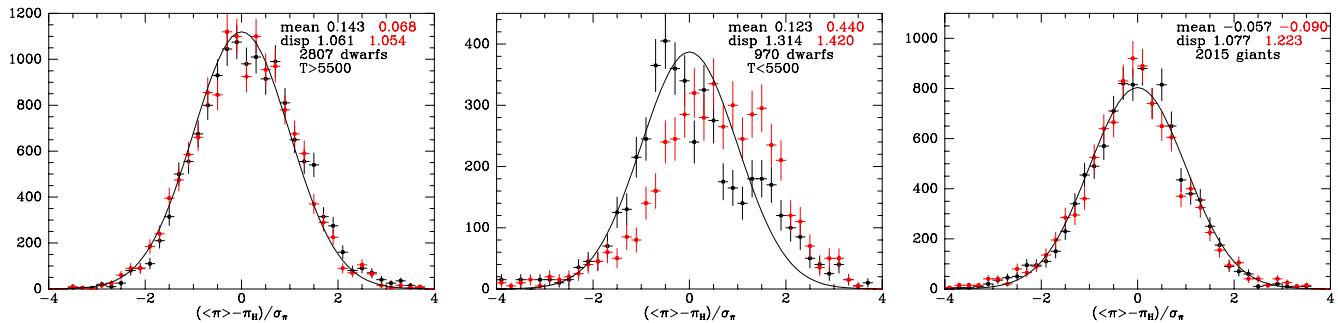

Figure 4. Histograms of the difference between spectrophotometric and *Hipparcos* parallaxes. The left-hand panel is for hot dwarfs, the centre panel is for cool dwarfs and the right-hand panel is for giants. The full curves are Gaussians of zero mean and unit dispersion, not fits to the data. The black points are obtained from the simple expectation of ϖ while the red points are obtained as described in the text from the Gaussian fits to the pdf in distance modulus. In these and subsequent histograms, the vertical axis plots dN/dx, the horizontal error bars mark the widths of the bins and the vertical error bars indicate Poisson uncertainties.

Table 4. Estimates of the external errors in the stellar parameters. The boundary between 'metal poor' and 'metal rich' lies at $[M/H] = -0.5$, and between 'hot' and 'cool' lies at 6000 K.

Stellar type	N	$\sigma(T_{\mathrm{eff}})$	$\sigma(\log g)$	$\sigma([M/H])$
		Dwarfs		
Hot, metal poor	28	314	0.466	0.269
Hot, metal rich	104	173	0.276	0.119
Cool, metal poor	97	253	0.470	0.197
Cool, metal rich	138	145	0.384	0.111
		Giants		
Hot	8	263	0.423	0.300
Cool, metal poor	273	191	0.725	0.217
Cool, metal rich	136	89	0.605	0.144

Table 5. Mean distance ratios for *Hipparcos* stars. Ideally, all entries would be unity.

	$\overline{\langle s \rangle / s_{\langle \mu \rangle}}$	$\overline{s_{\langle \mu \rangle} \langle \varpi \rangle}$	$\overline{\langle \varpi \rangle / \varpi_{\mathrm{H}}}$	$\overline{\langle s \rangle \varpi_{\mathrm{H}}}$
Hot dwarfs	1.045	1.040	0.958	1.042
Cool dwarfs	1.116	1.094	1.132	1.447
Giants	1.111	1.093	1.115	1.386

are easily understood in terms of the weights that each estimator attaches to possibilities of long or short distances. The comparison with the *Hipparcos* parallaxes clearly indicates that for stars with wide distance pdfs (cool dwarfs and giants), $1/\langle \varpi \rangle$ performs much better than either $\langle s \rangle$ or $s_{\langle \mu \rangle}$.

The red points Fig. 4 show histograms of discrepancies between the *Hipparcos* parallaxes and parallaxes based on the multi-Gaussian fits to the distance moduli as follows. When a single Gaussian has been fitted, we convert the mean and dispersion of this Gaussian into a parallax and its error by standard formulae. If two or three Gaussians have been fitted, we choose the Gaussian that makes the *Hipparcos* parallax most probable and convert the mean and dispersion of this Gaussian to a parallax and its error as before.

Table 5 gives these ratios for hot dwarfs, cool dwarfs and giants. For the hot dwarfs all ratios are pleasingly close to unity, but for both the cool dwarfs and the giants we see that $\langle s \rangle$ gives a systematically larger distance than $s_{\langle \mu \rangle}$, which in turn gives a bigger distance than $1/\langle \varpi \rangle$, which itself gives a bigger distance than $1/\varpi_{\mathrm{H}}$, which we take to be the most reliable distance estimator. These biases

The red histogram for the hot dwarfs is an almost perfect realization of the unit Gaussian while that for the giants is only marginally less satisfactory than the corresponding black histogram. The red histogram for the cool dwarfs is both significantly displaced to the right and broader than it should be.

Fig. 5 clarifies the situation by splitting the histogram of the cool dwarfs into those with pdfs that have been fitted with a single Gaussian (lower panel) and those with multi-Gaussian fits (upper panel). We see that for the latter stars the crude mean of possible parallaxes is smaller than it should be, and a more satisfactory distribution of spectrophotometric parallaxes is obtained if *Hipparcos* is used to choose between the Gaussians. The lower panel in Fig. 5 shows that when a cool dwarf has a single-Gaussian pdf, its parallax is systematically overestimated. When the single- and multi-Gaussian samples are aggregated in Fig. 4, the overestimated parallaxes of the single-Gaussian stars combine with the underestimated parallaxes of the multi-Gaussian stars to produce a deceptively satisfactory black histogram. The mean S/N of the *Hipparcos* stars with single-Gaussian fits is lower than that of the stars with multi-Gaussian fits (51.0 versus 66.5), so one suspects that with poorer data the system loses track of the possibility that the star has left the main sequence.

We test the soundness of the probabilities assigned to each Gaussian component of the pdf by calculating the sums $s_k = \sum_{\text{stars}} 1/f_k$, where $k = 1, 2, 3$ depending on which Gaussian component the *Hipparcos* data points to, and f_k is the weight of that component. Given a large sample of stars with accurate parallaxes (so the true component is always chosen), s_k should be independent of k because when f_k is small, that component will be rarely chosen so s_k will have a small number of large contributions, while a component with large f_k will be chosen often, but each contribution to s_k will be modest. When we compute mean values of $1/f_k$ for our *Hipparcos*
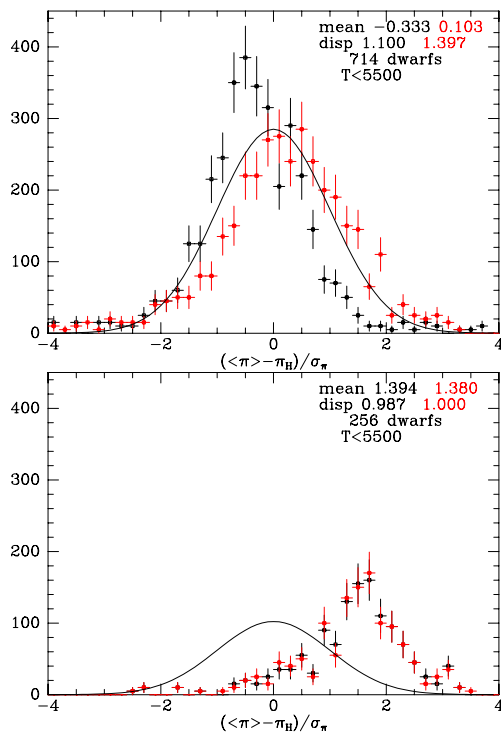
stars, we find 441/2807 hot dwarfs with two Gaussians fitted, and for these stars we find $s_k = (444, 458)$. Similarly, 615/970 cool dwarfs have two Gaussians and for these stars we find $s_k = (577, 2100)$, while 100 cool dwarfs have three Gaussians and for these stars $s_k = (94, 126, 476)$. 934/2015 giants have two Gaussians and these stars yield $s_k = (779, 3593)$ while 492 giants have three Gaussians and for these stars $s_k = (350, 759, 748)$. These results suggest that the probabilities assigned to the various Gaussians are broadly correct although there is a tendency for too little probability to be assigned to the weakest components.

The likely explanation of the neglect of weaker components is that the *Hipparcos* stars are biased towards nearer stars because stars thought to be near, usually on account of having large proper motions, preferentially entered the Hipparcos Input Catalogue. Consequently, we have tested the constancy of the s_k for a sample in which distant options will have been rather rarely chosen. For the giants the distant option is the more probable one, so it is natural that for these stars *Hipparcos* chooses the less probable Gaussian more often than one would expect if we had parallaxes for every star in our sample.

Fig. 6 shows the effect of setting $A_V = 0$ for all stars. With reddening neglected, dwarfs must be moved to lower masses to match the observed colours, and the consequent diminution of their luminosities causes them to be brought closer to match the observed magnitudes. The overall effect is to increase the spectrophotometric parallaxes of hot dwarfs by $\sim 0.05\sigma$, so those of the hot dwarfs are now on average too large by $\sim 0.19\sigma$, while those of the cool dwarfs are too large by $\sim 0.14\sigma$. With extinction neglected, giants need to be moved away to diminish their brightnesses so their histogram of $\langle \varpi \rangle - \varpi_H$ moves leftwards, and our parallaxes become too small by 0.12σ on average. Thus, the *Hipparcos* stars convincingly validate our procedure for taking into account the effects of dust.

Fig. 7 compares the distribution in the fractional errors in *Hipparcos* parallaxes (shown in green) with the corresponding errors in our parallaxes: the black points are for the straightforward expectation values of ϖ while the red points are for the parallaxes computed from the multi-Gaussian fits to the pdfs in distance modulus. For hot dwarfs, the black and red histograms are similar because few of these stars have multimodal pdfs. They show error distributions that are materially narrower than that from *Hipparcos*, with most values of $\sigma_\pi / \langle \varpi \rangle$ falling in the range $(0.18, 0.38)$ with a median value of 0.26.

For the cool dwarfs, the black and red histograms are quite different in that the red histogram shows a substantial population with spectrophotometric parallaxes in error by less than 10 per cent and essentially no stars with errors greater than 35 per cent. The stars with $\sigma_\varpi / \langle \varpi \rangle < 0.1$ are stars that the spectrophotometry cannot securely assign to dwarfs or giants until astrometric data become available – in the present case a *Hipparcos* parallax. There will probably be many stars of this type in the *Gaia* Catalogue. The red histogram for the giants shows a similar if smaller population of stars.

For now we must live with dwarf/giant confusion, and the black histograms of parallax errors are most relevant. These show that the spectrophotometric parallaxes of cool dwarfs are not competitive with *Hipparcos* parallaxes, in contrast to the case of some hot dwarfs and a number of giants, which do have more precise spectrophotometric parallaxes than *Hipparcos* parallaxes. Thus, the competitiveness of the spectrophotometric parallaxes vis-à-vis *Hipparcos* parallaxes increases along the sequence cool dwarfs to hot dwarfs to giants in parallel with the increase in the luminosities and thus typical distances of these stars.
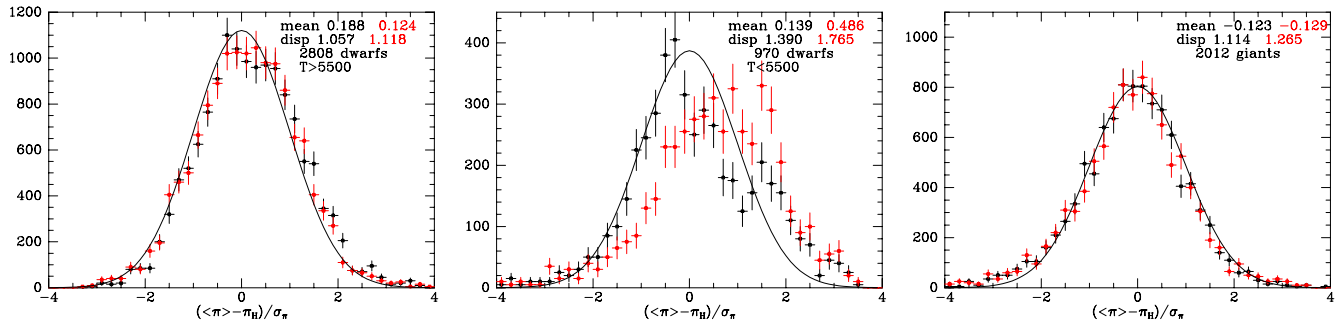

Figure 5. The centre histogram of Fig. 4 broken down into cold dwarfs with single-Gaussian (lower) and multiple-Gaussian (upper) pdfs.

Figure 6. Histograms of the difference between the *Hipparcos* parallaxes and expectation of the parallax from the spectrophotometry for hot dwarfs (left), cool dwarfs (centre) and giants (right) when the extinction is assumed to be zero. The full curves are Gaussians of zero mean and unit dispersion.
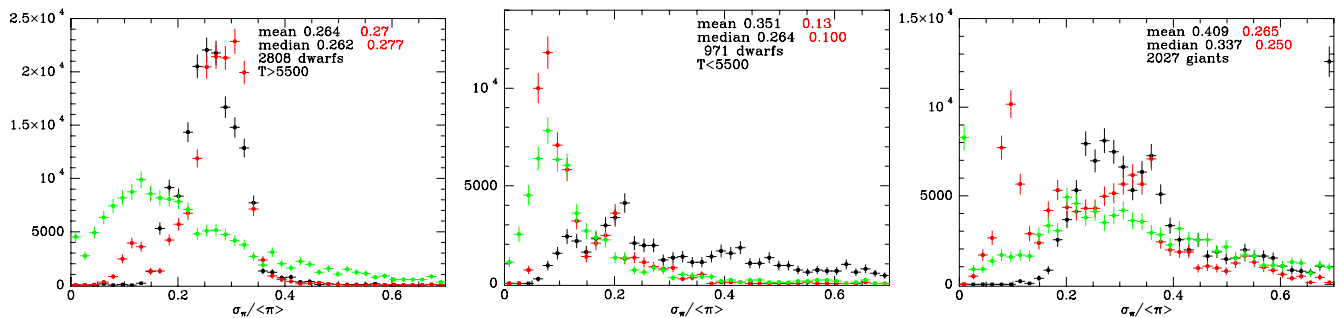

Figure 7. The distributions of errors in *Hipparcos* parallaxes (green) and in our spectrophotometric parallaxes (black and red) for hot dwarfs (left), cool dwarfs (centre) and giants (right). The black points show the errors in $\langle \varpi \rangle$ computed directly. The red points show the errors in parallaxes derived from the Gaussian fits to the pdf in distance modulus.

5 DISTANCES TO ALL STARS

We have examined the statistics of distances to RAVE stars as functions of a cutoff in the S/N of the analysed spectrum and found that the dependence on the cutoff S/N is weak. Below we report results obtained for stars with S/N $\geq$ 10 – the mean S/N for such stars that lie closer than 1.3 kpc is 33.

We have investigated the sensitivity of our distances to the model of the disc used in the prior (equations 3 and 4) by re-evaluating the distances to every 20th star in the catalogue with the scaleradii and scaleheights of both discs multiplied by a factor 1.5. The resulting histogram of ratios $\langle \varpi \rangle_2 / \langle \varpi \rangle_1$ of the parallax with the revised prior to the parallax with the standard prior peaks sharply at 1.02 but has a long tail to values ~1.2 with the consequence that the mean of this ratio is 1.045. This result shows that, as one would hope, our results are not sensitive to the prior.

Table 6 shows the ratios of the available distance measures for ordinary stars, broken down into giants and dwarfs, with the giants subdivided into stars with lower surface gravity than the red clump ($1.7 < \log g < 2.4$ and $0.55 \leq J - K \leq 0.8$), the red clump itself and stars with higher gravities. We see that in every case the distances are ordered $\langle s \rangle > s_{\langle \mu \rangle} > 1/\langle \varpi \rangle$. Moreover, $\langle s \rangle$ and $1/\langle \varpi \rangle$ are discrepant at the 26 per cent level for the highest gravity giants and coolest dwarfs, while for moderately cool dwarfs these measures are discrepant at the 17 per cent level.

5.1 Kinematic distance corrections

Schönrich et al. (2012a, hereafter SBA) describe a technique that uses the kinematics of stellar populations to identify and correct systematic errors in distances, and we can use this technique to determine which of our discrepant distance estimates is most reli-

Table 6. Ratios of distance measures for general stars with $s < 2$ kpc.

	$N_\star$	$\overline{\langle s \rangle / s_{\langle \mu \rangle}}$	$\overline{s_{\langle \mu \rangle} \langle \varpi \rangle}$	$\overline{\langle s \rangle \langle \varpi \rangle}$
Giants ($\log g < 3.5$)				
$\log g > 2.4$	69 008	1.11	1.13	1.26
Red clump	39 900	1.04	1.04	1.09
$\log g < 1.7$	28 472	1.06	1.05	1.11
Dwarfs ($\log g \geq 3.5$)				
$T_{eff} > 6500$	22 701	1.04	1.03	1.07
$5500 < T_{eff} \leq 6500$	71 641	1.04	1.04	1.08
$5200 < T_{eff} \leq 5500$	19 697	1.08	1.08	1.17
$T_{eff} \leq 5200$	27 408	1.13	1.12	1.29

able, and potentially to correct the most reliable measure for any systematic bias.

The corrections of SBA are based on the assumption that one knows roughly how the velocity ellipsoid is oriented at each point in the Galaxy, and that the only mean-streaming motion is azimuthal circulation at a speed $v(R, z) = \Theta g(R, z)$, where Θ is an unspecified constant and $g(R, z)$ is a function one chooses. We adopt

$$g = \sqrt{1 - (2\psi/\pi)^2}, \text{ where } \psi \equiv \arctan(z/R), \qquad (19)$$

which has an appropriate form, but the results are very insensitive to the choice of g: essentially unchanged results are obtained with $g = 1$. The algorithm involves converting heliocentric velocities to Galactocentric velocities and thus requires assumptions regarding the Galactocentric velocity of the Sun and the distance R_0 to the Galactic Centre. We assume that $R_0 = 8.33$ kpc, that the local circular speed is $\Theta_0 = 230$ km s^{-1} and that the Sun's velocity
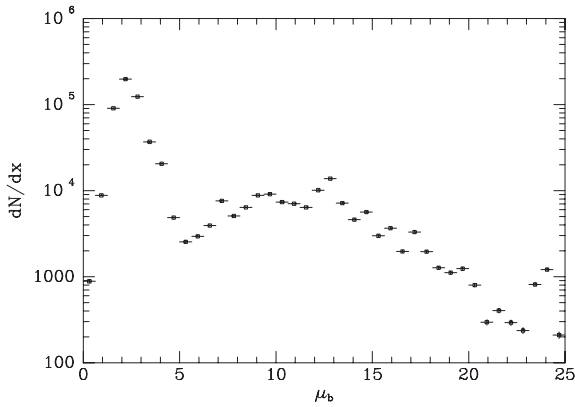
Figure 8. Histogram of the errors in the component μ_b of proper motion for all RAVE stars. The long tail of errors in excess of 8 mas yr^{-1} gives rise to nonsensical results, so we drop stars with such large proper-motion errors from the sample.

Table 7. Kinematic correction factors for general stars at $s < 2$ kpc. The first two columns give results of a test in which all stars were recorded to be further from the Sun than their true locations by a factor of 1.3. The last two columns are computed from the real RAVE catalogue.

	$f_W(T)$	$f_U(T)$	f_W	f_U
Giants (log $g < 3.5$)				
log $g > 2.4$	0.304	0.323	0.134	0.248
Red clump	0.311	0.332	0.160	0.249
log $g < 1.7$	0.310	0.348	0.453	0.676
Dwarfs (log $g \geq 3.5$)				
$T_{\rm eff} > 6500$	0.295	0.295	−0.270	−0.210
$5500 < T_{\rm eff} \leq 6500$	0.312	0.312	−0.081	−0.037
$5200 < T_{\rm eff} \leq 5500$	0.286	0.286	−0.064	−0.027
$T_{\rm eff} \leq 5200$	0.306	0.306	−0.026	0.043

with respect to the local standard of rest is $(U_0, V_0, W_0) = (11.1, 12.24, 7.25)$ km s^{-1} (Schönrich, Binney & Dehnen 2012b). There is very little sensitivity to the value of Θ_0. The azimuthal direction is assumed to be a principal axis of the velocity ellipsoid, while the latter's longest axis is tilted with respect to the plane by angle $\beta = a_0 \arctan(z/R)$, where a_0 is a parameter.

The corrections exploit pattern on the sky of correlations between the local Cartesian velocity components U, V, W that are introduced by distance errors. To assess the magnitude of these correlations, one has first to correct the raw correlations for contributions from sources other than distance errors. The most important such source is observational errors in the proper motions, so knowledge of the magnitude of these errors is needed for the correction.

Proper motions for RAVE stars can be drawn from several catalogues. Williams et al. (2013) compare results obtained with different proper-motion catalogues, and on the basis of this discussion we decided to work with the PPMX proper motions (Röser et al. 2008) because these are available for all our stars and they tend to minimize anomalous streaming motions. Fig. 8 shows a histogram of the errors for RAVE stars given in the PPMX catalogue. It shows that there is a fat tail in the error distribution, and one may show that this tail should not to be taken at face value because when one calculates the velocity dispersions of all the RAVE stars in spatial bins that are further than ∼0.5 kpc from the Sun, the dispersions are often smaller than the contribution expected from proper-motion errors alone. This paradox disappears if one cuts stars with errors in one component of proper motion greater than 8 mas yr^{-1}, and we impose this cut throughout the SBA analysis. The only class of stars that is significantly depleted by this cut is that of the very cool dwarfs, which shrinks from 38 330 stars to 27 332 stars. This cut reduces the rms error in one component of proper motion to 2.5 mas yr^{-1}.

A second source of correlations that complicate the SBA analysis is rotation of the velocity ellipsoid's principal axes as one moves around the Galaxy, and a model of the velocity ellipsoid is used to correct for this effect. The final product is the factor $1 + f$ by which all distances must be contracted (or expanded if $f < 0$) for all correlations between U, V and W to be accounted for by a combination of observational errors and rotation of the principal axes of the velocity ellipsoid.

SBA give two formulae for corrections, one, f_U, involving 'targeting' U and one, f_W, using W as a target. Because the latter is independent of azimuthal streaming, it is the simpler and more reliable. Their equations 19 and 38 give the W and U correction factors, respectively, after the raw covariances have been corrected for observational errors using their equations 22 and 25.

From the RAVE data, we have extracted correction factors to the distance estimator $1/\langle \varpi \rangle$ for the three types of giants and four types of dwarfs listed in Table 6. The code used to determine the corrections was tested as follows. For each star in a class, the measured U, V, W velocities were replaced by values chosen from a triaxial Gaussian velocity ellipsoid that has dispersions $\sigma_i = (40, 40/\sqrt{2}, 30)$ km s^{-1} around systematic rotation at 200 km s^{-1}. Most tests were run with the orientation of the principal axes determined by setting $a_0 = 0.8$, but excellent results are obtained with other plausible values of a_0, including zero. Likewise, the outcome of the code tests is not sensitive to the adopted dispersions σ_i. Next proper motions and line-of-sight velocities are calculated from the model velocities, and Gaussian observational errors are added with the dispersions that are given in the PPMX catalogue. Then the stars are moved along their lines of sight to points more distant by a factor $1 + f$, and their U, V, W components are re-evaluated from the proper motions. In this way, we obtain a catalogue of phase-space positions for a population of objects whose distances have been overestimated by a factor $1 + f$. The SBA algorithms are then used to infer the value of f from this catalogue.

The first two numerical columns of Table 7 show the fractional distance excesses f_W and f_U obtained by targeting W and U when distances to the stars have been overestimated by a factor $1 + f$ with $f = 0.3$. Consequently, ideally we would have $f_W = f_U = 0.3$ for all star classes. For f_W this expectation is borne out for all classes to better than 5 per cent, and for the dwarfs it is similarly for f_U. For the giants, f_U is up to 16 per cent larger than it should be, a result which reflects the breakdown of the approximations made by SBA when dealing with more distant stars.

The final two columns of Table 7 show the fractional distance excesses f_W and f_U for the seven classes of RAVE stars using the measured distances and velocities when $1/\langle \varpi \rangle$ is used as the distance measure. For the giants, the differences between f_W and f_U are in the same sense ($f_U > f_W$) as in the tests but they are larger than those in the tests. The cause of this difference is not obvious, but one suspects a major contributor is the well-known existence of clumps of stars in the (U, V) plane (Dehnen 1998; Famaey et al. 2005; Antoja et al. 2012), which conflict with the assumption of simple azimuthal streaming that is fundamental to SBA's derivation of the formula for f_U. Since prominent clumps are absent from the distribution of *Hipparcos* stars in the (U, W) and (V, W) planes (Dehnen

Table 8. Kinematic correction factors for general stars at $s < 1.3$ kpc. The first two columns report results from a test in which the recorded locations of stars were further than their true locations by a factor $1 + f$, where f is a random variable with mean and dispersion 0.2.

	$f_W(T)$	$f_U(T)$	f_W	f_U
Giants ($\log g < 3.5$)				
$\log g > 2.4$	0.203	0.203	0.066	0.185
Red clump	0.157	0.157	0.114	0.148
$\log g < 1.7$	0.100	0.130	0.210	0.334
Dwarfs ($\log g \geq 3.5$)				
$T_{\rm eff} > 6500$	0.220	0.207	-0.270	-0.210
$5500 < T_{\rm eff} \leq 6500$	0.217	0.217	-0.081	-0.037
$5200 < T_{\rm eff} \leq 5500$	0.227	0.247	-0.064	-0.027
$T_{\rm eff} \leq 5200$	0.217	0.217	-0.050	0.041

1998), f_W is expected to be a more reliable diagnostic of distance errors than f_U. Table 7 then suggests that $1/\langle \varpi \rangle$ overestimates distances to high-gravity giants and red clump stars by ~ 15 per cent, and gives distances to dwarfs that are too small by factors that rise from ~ 5 per cent at the cool end to ~ 25 per cent at the hot end.

In selecting stars for inclusion in the SBA analysis, we have imposed a limit $s_{\rm max}$ on the reported distance, and the results one obtains for both the test and with the real data depend on the value chosen for $s_{\rm max}$. Table 7 is based on the choice $s_{\rm max} = 2$ kpc. Table 8 is based on $s_{\rm max} = 1.3$ kpc, and the results of tests reported in the first two numerical columns of this table differ from those reported in the corresponding columns of Table 7 in that the distances to stars were increased by a factor $1 + f$, where f is now a Gaussian random variable with mean and dispersion 0.2. The test results are fairly satisfactory for the dwarfs in that both f_W and f_U have values within ~ 10 per cent of the true value, 0.2. The test results for the giants are decidedly less satisfactory in that the f values are too small by an amount which increases with the typical luminosity within a class. It is easy to understand why this is so: stars that happen to get a large fractional distance increase are liable to be pushed beyond $s_{\rm max}$ whilst stars that have their distances decreased can enter the sample from beyond $s_{\rm max}$, and the SBA algorithm correctly infers

that on average the stars *in the analysed sample* have small distance overestimates even though in the population as a whole stars have larger distance overestimates. Clearly, for this phenomenon to be important, the catalogue needs to contain many stars that really are at distances $\sim s_{\rm max}$. The dwarfs do not satisfy this condition, but the low-gravity giants very much straddle the 1.3 kpc distance cut.

Comparing columns 3 and 4 of Table 8 with the corresponding columns of Table 7, we see that reducing $s_{\rm max}$ from 2 to 1.3 kpc has only a modest effect on the f values for dwarfs and a significant effect on giants. The f values of giants decrease significantly for all three classes, but the final f_W factors still increase with decreasing gravity contrary to the tendency seen in the test, so we really must be overestimating distances to the lowest gravity (and most luminous) giants. A possible explanation is that we are using stellar parameters obtained under the assumption of local thermodynamic equilibrium (LTE). The validity of LTE decreases with $\log g$, and when non-LTE effects are taken into account, the recovered gravity of a giant star increases (Ruchti et al. 2013), and the predicted luminosity decreases, bringing the star closer.

The squares in Fig. 9 show the values of $1 + f_W$ obtained when the giants are grouped by $\log g$ and the dwarfs are grouped by $T_{\rm eff}$ – in each case the SBA algorithm is used on 15 bins of stars at $1/\langle \varpi \rangle < 1.3$ kpc with equal numbers of stars in each bin, and all bins are statistically independent. The triangles show the analogous ratios $\varpi_{\rm H}/\langle \varpi \rangle$ of our distance to that implied by the *Hipparcos* parallax. The curves show fifth-order polynomial fits to all the points. The squares and triangles tell the same story from a qualitative perspective: along the sequence of giants, there is a steady increase in the tendency to overestimate distances as one moves to lower gravity (and higher luminosity), while the dwarfs show a clear trend towards distance overestimation with falling $T_{\rm eff}$ with the exception of the coolest bin, which shows marked distance underestimates. The SBA points for dwarfs tend to lie below those from *Hipparcos*, so SBA and *Hipparcos* disagree about the value of $T_{\rm eff}$ at which our distances are unbiased.

Our tests suggest that f_W should be a reliable guide to any systematic errors in the distances to our dwarf stars. The situation regarding the giant stars is less clear because the f values are biased low unless $s_{\rm max}$ is large enough to encompass most of the stars in the catalogue. Unfortunately, the more distant the stars, the more
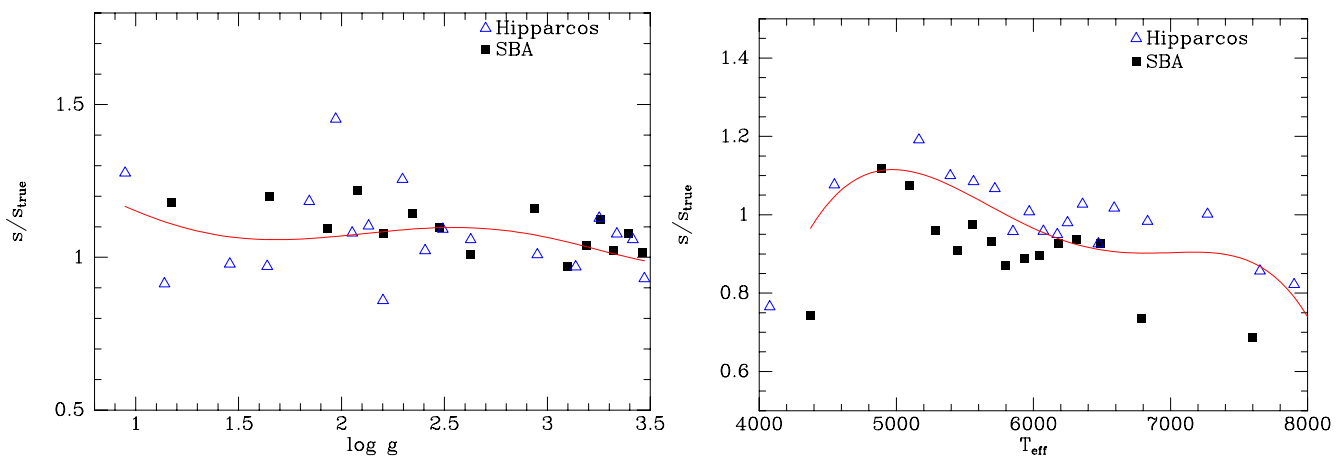

Figure 9. The squares show the ratios $1 + f_W$ of the spectrophotometric distances $1/\langle \varpi \rangle$ to the true distances for giants with $1/\langle \varpi \rangle < 1.3$ kpc broken down by $\log g$ (left) and dwarfs broken down by $T_{\rm eff}$ (right). All bins contain the same number of stars, and each star is in only one bin so the data points are mutually independent. The triangles show the same quantities inferred for *Hipparcos* stars from their directly measured parallaxes, again using equally populated and independent bins. The red curve shows fifth-order Chebyshev polynomials fitted to all the data.

sensitive the returned value of f_U becomes to restrictive assumptions regarding the pattern of mean-streaming and random velocities in the Galaxy and some approximations. The value of f_W is less sensitive to these issues and therefore more reliable, but its sensitivity to s_{max} is worrying. A further blow to the credibility of f_W will emerge below from an analysis of the red clump stars.

5.1.1 Kinematic corrections to multi-Gaussian pdfs

SBA assume that one is working with a simple distance estimator, while in Section 3 we saw that our most complete information is contained in a distance pdf. Can we use a kinematic analysis to refine these pdfs?

The SBA algorithm involves several sample averages such as $\langle Wy \rangle$, where W and y are quantities that depend on the distance to each star. In our analysis above, we evaluated these for just one distance, but given a pdf $P(\mu)$ it is straightforward to replace Wy by the expectation value of Wy:

$$\overline{Wy} \equiv \int \mathrm{d}\mu \, P(\mu) W(\mu) y(\mu). \tag{20}$$

These expectation values are then averaged over the sample to produce the sample averages $\langle Wy \rangle$, etc., that appear in the SBA formalism. Thus, it is straightforward to use the pdfs to calculate a kinematic correction factor such as f_y.

It is less clear how one should modify the pdf in light of a non-zero value of f_y. We have experimented with two possibilities.

(i) Move the centres of all the Gaussians to larger or smaller distance moduli until $f_y = 0$. This procedure produces results that are rather similar to, but slightly less convincing than, those obtained without the pdfs.

(ii) When a star has more than one Gaussian in its pdf, modify the probabilities f_k (equation 14) associated with the two most probable Gaussians. This procedure is appropriate if the Bayesian algorithm has correctly identified the two model stars that an observed star could be, but, perhaps driven by a faulty prior, has assigned inappropriate odds to the options. We now report results obtained with this procedure.

We make the probabilities f_1 and f_2 in equation (14) a function of a variable θ through

$$f_1 = A\cos^2(\theta), \quad f_2 = A\sin^2(\theta), \tag{21}$$

where at the outset we fix $A \equiv f_1 + f_2$ to be the total probability associated with the two most probable options. Then we make θ, which is confined to the range $(0, \pi/2)$, a function of a variable ξ that can span the whole real line, through

$$\theta = \arctan(e^\xi). \tag{22}$$

The original values of f_i determine starting values for θ and ξ. If the kinematic analysis has returned $f_y > 0$, implying that distances need to be shortened and the first Gaussian describes a nearer option than the second, then we lower θ by subtracting $5f_y$ from ξ – the factor 5 is arbitrary: smaller values lead to slower convergence of the iterations but larger values can cause the iterations to undergo diverging oscillations. If, conversely, $f_y < 0$, we need to increase θ and ξ so we add $5f_y$ to ξ.

Table 9 shows results obtained by iterating up to six times or until $|f_y| < 0.01$. The first numerical column gives the mean of $|\xi|$ for all stars that have more than one Gaussian. A value greater than ~ 3 implies that all available probability has been driven into whichever Gaussian will reduce $|f_y|$. For the giants, this condition is reached

Table 9. Kinematic corrections to the pdfs. A large average value of the parameter ξ defined by equation (22) implies that all the probability has been driven into one Gaussian. The second and third numerical columns give the initial and final values of the kinematic error estimator, which is ideally zero.

	$\overline{|\xi|}$	$f_y(\mathrm{i})$	$f_y(\mathrm{f})$
Giants ($\log g < 3.5$)			
$\log g > 2.4$	2.16	0.403	0.004
Red clump	24.85	0.906	0.858
$\log g < 1.7$	5.55	0.290	0.134
Dwarfs ($\log g \geq 3.5$)			
$T_{\mathrm{eff}} > 6500$	8.22	-0.252	-0.247
$5500 < T_{\mathrm{eff}} \leq 6500$	0.39	-0.015	-0.009
$5200 < T_{\mathrm{eff}} \leq 5500$	0.55	0.030	0.004
$T_{\mathrm{eff}} \leq 5200$	1.99	0.247	0.005

after about four iterations and is signalled by successive values of f_y becoming nearly identical. The second column gives the initial value of f_y and the third column gives the value of f_y at the end of the iterations. We see that in the case of the highest gravity giants, adjusting the f_i has reduced f_y to the target value, but that there is insufficient ambiguity in the nature of the clump stars and the low-gravity giants to get f_W below the target value.

There is very little ambiguity in the nature of the hottest dwarfs, so the procedure makes no significant progress in eliminating the tendency for their distances to be underestimated.

The procedure succeeds with the remaining dwarfs: for all three classes, $|f_y|$ is reduced to below the target value, and the modest values of $\overline{|\xi|}$ given in the first numerical column show that this is achieved without driving all the probability into one option.

From this analysis, we conclude that there is sufficient ambiguity in the nature of stars that are cooler that $T_{\mathrm{eff}} = 5500\,\mathrm{K}$ and have $\log g > 2.4$ to account for non-zero values of the SBA factor f_W but too little ambiguity in the nature of hotter dwarfs and low-gravity giants to account for non-zero f_W.

5.2 Absolute magnitude of the red clump

Helium-burning stars in the red clump have frequently been used as standard candles (e.g. Cannon 1970; Pietrzynski, Gieren & Udalski 2003). Recently, Williams et al. (2013) used clump stars in the RAVE survey to analyse the velocity field around the Sun, and reviewed our knowledge of the absolute magnitudes of these objects and the possibility that they depend on age and metallicity. They identified 78 019 clump stars as those satisfying the cuts $0.55 \leq J - K \leq 0.8$ and $1.8 \leq \log g \leq 3$, where $\log g$ was taken from the vDR3 pipeline (Siebert et al. 2011). We use the same colour range but a narrower band (1.7, 2.4) in $\log g$ and with gravity taken from the vDR4 pipeline (Kordopatis et al. 2013).

Fig. 10 shows the distributions of H- and K-band absolute magnitudes for distance $1/\langle \varpi \rangle$ of clump stars. The distributions are satisfyingly narrow – each has a standard deviation of 0.20 mag – but they are skew, so while their means lie at $M_H = -1.39$ and $M_K = -1.49$ their peaks lie at $M_H = -1.42$ and $M_K = -1.53$. These magnitudes are in the SAAO system: using the formulae of Koen et al. (2007) to convert to the 2MASS system, we find the mean of M_K to be $M_K = -1.51$. The sample was restricted by $1/\langle \varpi \rangle < 1.3\,\mathrm{kpc}$, but increasing the distance cutoff to 2 kpc only changes the mean
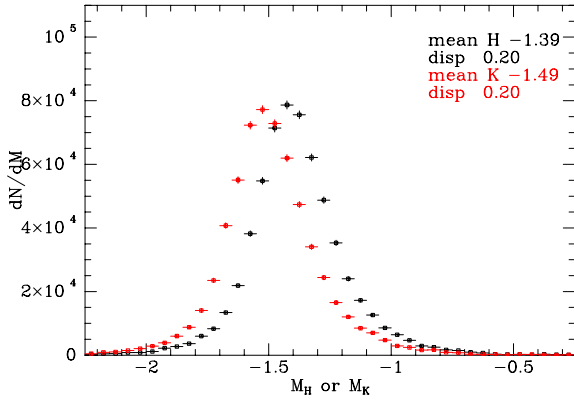
Figure 10. The distribution of absolute *H* and *K* magnitudes of red clump stars with $1/\langle\varpi\rangle < 1.3\,\mathrm{kpc}$.

absolute magnitudes to $M_H = -1.36$ and $M_K = -1.46$. For comparison, Laney, Joner & Pietrzynski (2012) determined $M_H = -1.49 \pm 0.022$ and $M_K = -1.61 \pm 0.022$ from a sample of 191 *Hipparcos* stars, and Williams et al. (2013) used calibrations in which the 2MASS absolute magnitudes were $M_K = -1.65, -1.54$ and $-1.64 + 0.0625z/\mathrm{kpc}$. In the last calibration, the decrease in luminosity with increasing distance from the plane reflects the expected increasing age and decreasing metallicity of clump stars. However, the age–metallicity sensitivity of the absolute magnitude is expected to be smallest in the *K* band (e.g. Salaris 2013). Several issues require discussion when considering why our values are ∼0.1 mag fainter than those of Laney et al.

(i) One might argue that the figures given above actually underestimate the scale of the conflict with Laney et al. (2012) (and many similar values in the literature) because we ought to have corrected our values for the systematic distance overestimates implied by the upper panel of Fig. 9. When this is done (using the red curve), we obtain $M_H = -1.21$ and $M_K = -1.32$; since we have moved the stars nearer, we conclude that they are less luminous.

(ii) The study of Laney et al. (2012) involved obtaining new *JHK* photometry for their *Hipparcos* stars because the 2MASS photometry of *Hipparcos* red clump stars, which have bright apparent magnitudes, is affected by saturation, which makes them appear fainter than they really are. Unfortunately, only four of our stars

were measured by Laney et al. For these stars, Laney et al. obtained *J* magnitudes brighter than the 2MASS values by amounts in the range (−0.006, 0.457), but their *H* and *K* values are not clearly brighter than the 2MASS values, which suggests that saturation in 2MASS is mainly confined to the *J* band. Interestingly, the Bayesian algorithm assigns an anomalous extinction ($A_V = 0.633$) to the star (Hipp 32222) that shows by far the strongest saturation effects, presumably because a high extinction can explain the unexpectedly faint *J* magnitude given the spectroscopically determined T_{eff}. From this rather fragmentary evidence, we infer that the effects of saturation on the 2MASS magnitudes might cause us to make the nearest clump stars underluminous by ∼0.1 mag. The triangles in Fig. 9 suggest on the contrary that we have found these stars to be overluminous by ∼0.4 mag.

(iii) Are the red clump stars in our sample correctly identified? Fig. 11 shows the density of stars in the $(J - K, \log g)$ plane for two metallicity ranges. In both panels, peaks in density are apparent near the theoretical locations of core helium-burning stars. These peaks are captured by our selection criteria $1.7 < \log g < 2.4$ and $0.55 \leq J - K \leq 0.8$. The core helium-burning model star that sits at the centre of the red circle has $T_{\mathrm{eff}} = 4485$, $\log g = 2.37$ and $M_K = -1.60$, in agreement with the empirical data of Laney et al. (2012).

This discussion explains why our raw distances imply absolute magnitudes for clump stars that differ little from the empirical value of Laney et al., and why these distances are only slightly larger than the *Hipparcos* parallaxes imply. The puzzle remains that the SBA kinematic analysis points to our distances being too large. For the SBA analysis to be correct, we would require *both* that the stellar models were too luminous *and* the *Hipparcos* stars to be misleading, perhaps because they are nearby and therefore anomalously young and have atypical chemistry. Consequently, we set the SBA correction factors aside for the moment, but in a companion paper (Binney et al. 2013) we will return to this issue in the context of dynamical Galaxy models.

Table 6 shows that $1/\langle\varpi\rangle$ is always the shortest of our distance measures, and given the suggestion from the SBA analysis that even this measure might be too long, we do not present an SBA analysis of distances based on $\langle s \rangle$ or $s_{\langle\mu\rangle}$. However, such analyses do confirm that these measures overestimate distances to all classes of star by even larger factors than $1/\langle\varpi\rangle$ does, so there is no case to be made for using them.
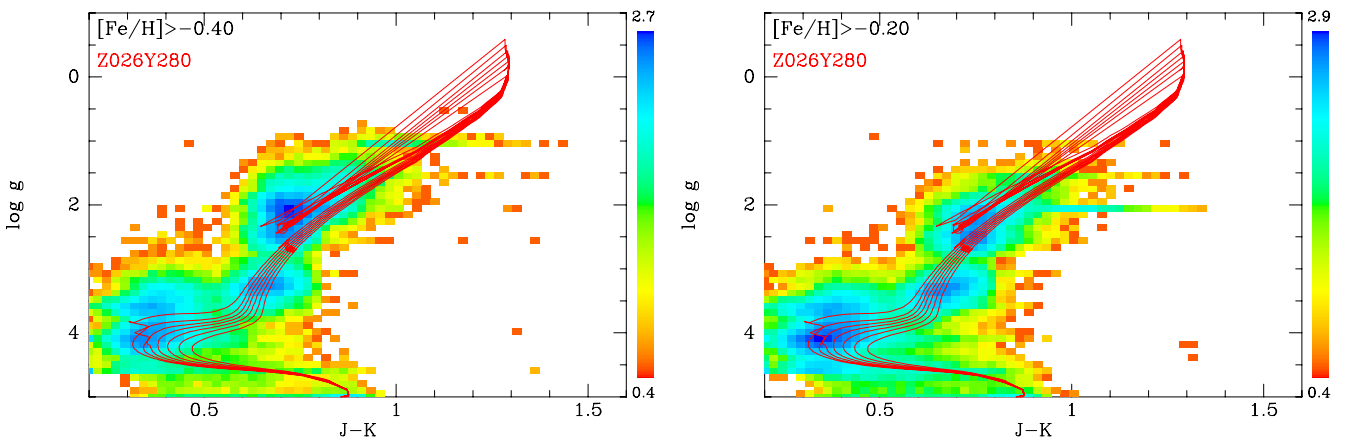

Figure 11. Density of stars on a logarithmic scale for two metallicity ranges in the $(J - K, \log g)$ plane together with Padova isochrones for metal-rich populations. The left-hand panel is for ($-0.4 < [\mathrm{Fe/H}] < -0.2$) and the right-hand panel is for ($-0.2 < [\mathrm{Fe/H}] < 0$).

5.3 Effective temperature–absolute magnitude diagrams

Fig. 12 shows effective temperature–absolute magnitude diagrams for high-latitude ($|b| > 40°$) stars created either (a) using $\langle\varpi\rangle$ to assign a single distance to each star (left-hand panel) or (b) spreading each star in M_K according to the multi-Gaussian fit to its pdf in distance modulus. The red octagon centred on $(T_{\rm eff}, M_K) = (5780, 3.28)$ shows the location of the Sun in the effective temperature–absolute magnitude diagram.

The red clump is prominent in both panels but the horizontal branch extends further to the blue when the pdfs are used as a consequence of eliminating the messy scatter of stars in the left-hand panel between the horizontal branch and the main sequence. Using the pdfs similarly eliminates the unphysical scatter of stars inside the turnoff curve. In both diagrams, vertical stripes are evident, especially at the coolest temperatures: these are a legacy of the use by the pipeline of the DEGAS decision-tree routine to identify template spectra (Kordopatis et al. 2013). This artefact is enhanced because we have smeared stars in M_K but not in $T_{\rm eff}$, as we should have done for consistency.

Fig. 13 shows effective temperature–absolute magnitude diagrams for two slices through the Galaxy: $|z| < 0.2$ kpc or $0.4 < |z|/\,{\rm kpc} < 0.9$. For these plots, we used the multi-Gaussian

representations of pdfs to spread stars in distance modulus and thus in z. At $|z| < 0.2$ kpc the main sequence, subgiant and giant branches show up nicely, and the red clump is extremely sharp. More than 0.4 kpc away from the plane the lower main sequence has disappeared and giant branch becomes more strongly populated because the volume surveyed is much larger.

6 CLUSTER STARS

By searching for stars that have suitable sky coordinates and line-of-sight velocities that agree with a cluster convergence point, we have identified RAVE stars in 15 open clusters. NGC 3680 has just one RAVE star so we cannot analyse its statistics. Table 10 lists the remaining clusters with RAVE stars in order of increasing age, giving for each cluster the values of several quantities from the literature. The values given are taken from Dias et al. (2002) with the exception of the Hyades, where we used Perryman et al. (1998).

Columns 7 and 8 give the number of giants in our sample and the ratio of their mean value of $1/\langle\varpi\rangle$ to the distance listed in Table 10. Columns 9 and 10 give the same data for dwarfs, and column 11 gives the overall mean of $1/\langle\varpi\rangle$ for cluster stars divided by the literature distance. A tendency for the giants to overestimate
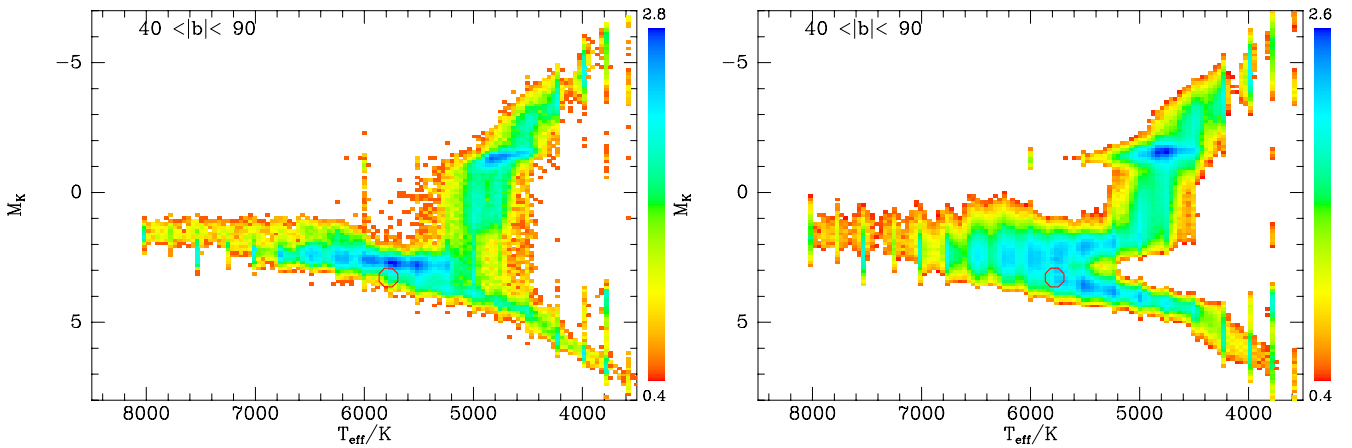

Figure 12. Effective temperature–absolute magnitude diagrams for $|b| > 40°$ either using for each star the absolute magnitude implied by the distance estimator $1/\langle\varpi\rangle$ (left) or spreading each star out in absolute magnitude according to the multi-Gaussian representation of its pdf in distance modulus (right). The density scale is essentially logarithmic: the quantity plotted is $\log_{10}(1 + n)$, where n is the number of stars in a cell. The red octagon is centred on the location of the Sun $(T_{\rm eff}, H) = (5780, 3.28)$.
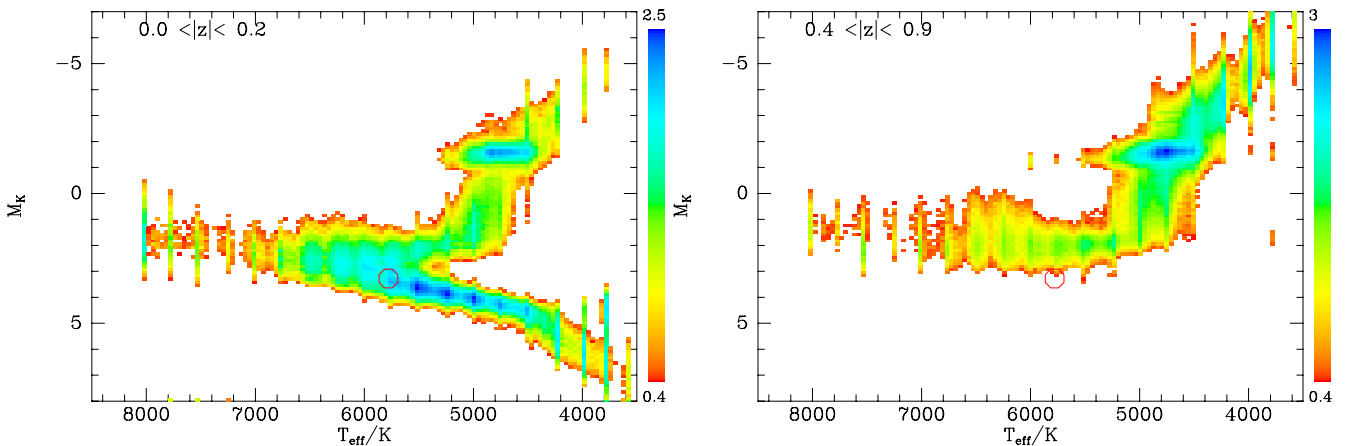

Figure 13. Effective temperature–absolute magnitude diagrams for two slices in $|z|$ constructed using the multi-Gaussian representations of stars' pdfs and using the same density scale as in Fig. 12.

Table 10. Analysis of cluster stars. σ_{cl} is the assumed cluster radius and $\log \tau$ gives the literature age while $\overline{\log \tau}$ is the mean logarithm of the inferred ages of cluster stars (in years) and s_{cl} is the literature value of the cluster distance (in pc). N_g and N_d are the numbers of giants and dwarfs in the sample and $\bar{s}_g$ and $\bar{s}_d$ are the mean distances to giants and dwarfs inferred from values of $1/\langle \varpi \rangle$. $\bar{s}_{all}$ is the mean distance of all cluster stars and is given also when extinction is neglected ($\bar{s}_{all,nE}$) and when a strong, cluster-specific age prior is used ($\bar{s}_{all,\tau}$).

Cluster	σ_{cl}	$E(B-V)$	$\log \tau$	$\overline{\log \tau}$	s_{cl}	N_g	$\bar{s}_g/s_{cl}$	N_d	$\bar{s}_d/s_{cl}$	$\bar{s}_{all}/s_{cl}$	$\bar{s}_{all,nE}/s_{cl}$	$\bar{s}_{all,age}/s_{cl}$
Blanco 1	5.5	0.01	7.80	9.59	269	4	1.61	23	1.07	1.15	1.13	0.87
NGC 2422	3.6	0.07	7.86	8.82	490	0	–	13	1.09	1.09	1.08	0.85
Alessi 34	15.4	0.18	7.89	9.58	1100	24	1.20	0	–	1.20	1.82	3.71
ASCC 69	14.0	0.17	7.91	9.51	1000	30	1.63	2	0.84	1.58	2.11	4.87
NGC 6405	2.8	0.14	7.97	8.89	487	0	–	12	0.94	0.94	0.90	0.71
Melotte 22 (Pleiades)	4.6	0.03	8.13	9.39	133	2	1.11	35	1.09	1.09	1.11	0.93
NGC 3532	7.1	0.04	8.49	8.95	486	1	1.71	17	1.23	1.26	1.24	0.97
NGC 2477 (M93)	5.7	0.24	8.78	9.29	1300	45	0.91	3	1.02	0.92	1.13	1.27
Hyades	5.7	0.01	8.80	9.70	46	0	–	31	1.08	1.08	1.08	1.00
NGC 2632 (Praesepe, M44)	3.8	0.01	8.86	9.48	187	0	–	34	1.14	1.14	1.12	1.03
NGC 2423	2.7	0.10	8.87	8.96	766	3	1.36	17	0.99	1.05	0.99	1.17
IC 4651	2.6	0.12	9.06	9.30	888	7	1.03	5	0.68	0.87	0.87	1.00
NGC 2682 (M67)	6.6	0.06	9.41	9.74	908	32	0.74	12	0.65	0.72	0.74	0.78

distances is evident, particularly in the younger clusters such as Alessi 34 and ASCC 69. The distances inferred for dwarfs are generally in good agreement with the literature values, but significant underestimates are evident in the cases of the oldest clusters, IC 1651 and NGC 2682 (M67). The penultimate column gives the mean value of $1/\langle \varpi \rangle$ divided by the literature distance when extinction is assumed to be zero. Setting $A_V = 0$ shortens distances to dwarfs and lengthens those to giants, and for a few clusters the results with no dust are markedly worse but neglecting dust has little impact on most clusters.

Column 5 gives the mean inferred value of the logarithm of age (in years), and comparing these values with the literature values in column 4 we see little sign of correlation with the result that stars in younger clusters are being presumed much older than they really are. This phenomenon reflects the fact that dating an isolated star is enormously harder than dating a cluster of coeval stars. Clearly, poor ages will bias the recovered distances, so in the last column of Table 10 we give the mean values of $1/\langle \varpi \rangle$ divided by the literature distance when distances are determined under the strong age prior

$$P(\tau) \propto \exp\left[-\log_{10}^2(\tau/\tau_{cl})/2(0.1)^2\right]. \tag{23}$$

This cluster-specific age prior improves the accuracy of mean distances to stars in clusters older than 100 Myr, but has an unfortunate effect on the distances to stars in younger clusters.

Fig. 14 shows histograms of distances to stars in 12 of the 13 clusters listed in Table 10; the red histograms are for our standard distances and the blue histograms are for distances obtained under the strong cluster-specific prior. The numbers in parentheses after the cluster names in the top-left corner of each panel give the number of giants and dwarfs in that cluster. The top panel of Fig. 15 shows the corresponding plot for NGC 2682 (M67). We see that the strong age prior shortens distances to dwarfs and lengthens those to giants in a way that is moderate and beneficial in clusters as old as the Melotte 22 (Pleiades) but unhelpful in younger clusters. The red histograms are generally quite satisfactory.

7 REPEAT OBSERVATIONS

We have more than one spectrum for 12 012 stars and can form 8526 independent pairs of measurements for the same dwarf star and 11 868 independent pairs of measurements for the same giant star. Fig. 16 shows histograms of the discrepancies between these

measurements when normalized in two ways. In the upper panel, the difference in $\langle \varpi \rangle$ is divided by the mean parallax, while in the lower panel it is divided by the quadrature sum of the uncertainties of the measurements. The median fractional parallax discrepancy is 0.063 for giants and 0.069 for dwarfs – it is easy to show that these values apply also to the discrepancies in distances $1/\langle \varpi \rangle$. The dispersions of the parallax discrepancies normalized by the formal uncertainties are 0.295 for giants and 0.348 for dwarfs. That these numbers are significantly smaller than unity emphasises that much of the error is external and does not derive from noise in the spectrum.

8 ESTIMATED EXTINCTIONS

As with distances, the Bayesian algorithm determines a probability distribution for possible extinctions to each star, and one has to consider how best to reduce this distribution to a single value for the extinction. For the reasons given in Section 2, the code marginalizes over extinctions by integrating with respect to $a \equiv \ln(A_V)$ rather than integrating with respect to A_V directly. Consequently, a natural quantity to output is $\langle a \rangle$, and we use $\widetilde{A}_V \equiv e^{\langle a \rangle}$ as our estimator of the extinction. $\widetilde{A}_V$ places less weight on high extinctions than does $\langle A_V \rangle$.

Fig. 17 shows that different spectra yield the same value for $\widetilde{A}_V$ to high precision: the dispersions in the differences divided by the quadrature sum of the uncertainties are only 0.117 for giants and 0.097 for dwarfs. This result is to be expected because $\widetilde{A}_V$ depends strongly on the photometry, and we only change the spectrum between determinations of $\widetilde{A}_V$.

Fig. 18 shows in red the distribution of extinctions to *Hipparcos* stars; the blue points show the distribution of the prior values of the extinction to the final locations $1/\langle \varpi \rangle$ of the stars. Since the red and blue points follow very similar distributions, on average our recovered extinctions coincide well with our priors. This finding could indicate either that our priors are accurate guesses of the actual extinction or that the extinction to an individual star cannot be determined from the data we have. We know that the data *are* adequate because when we took the priors from the smooth model (11) normalized in an average sense by the Schlegel et al. reddenings, the recovered values of $\widetilde{A}_V$ were systematically smaller than the prior values. Thus, the data suffice to shift the recovered values away from a poor prior. Presumably, the *Hipparcos* stars lie in
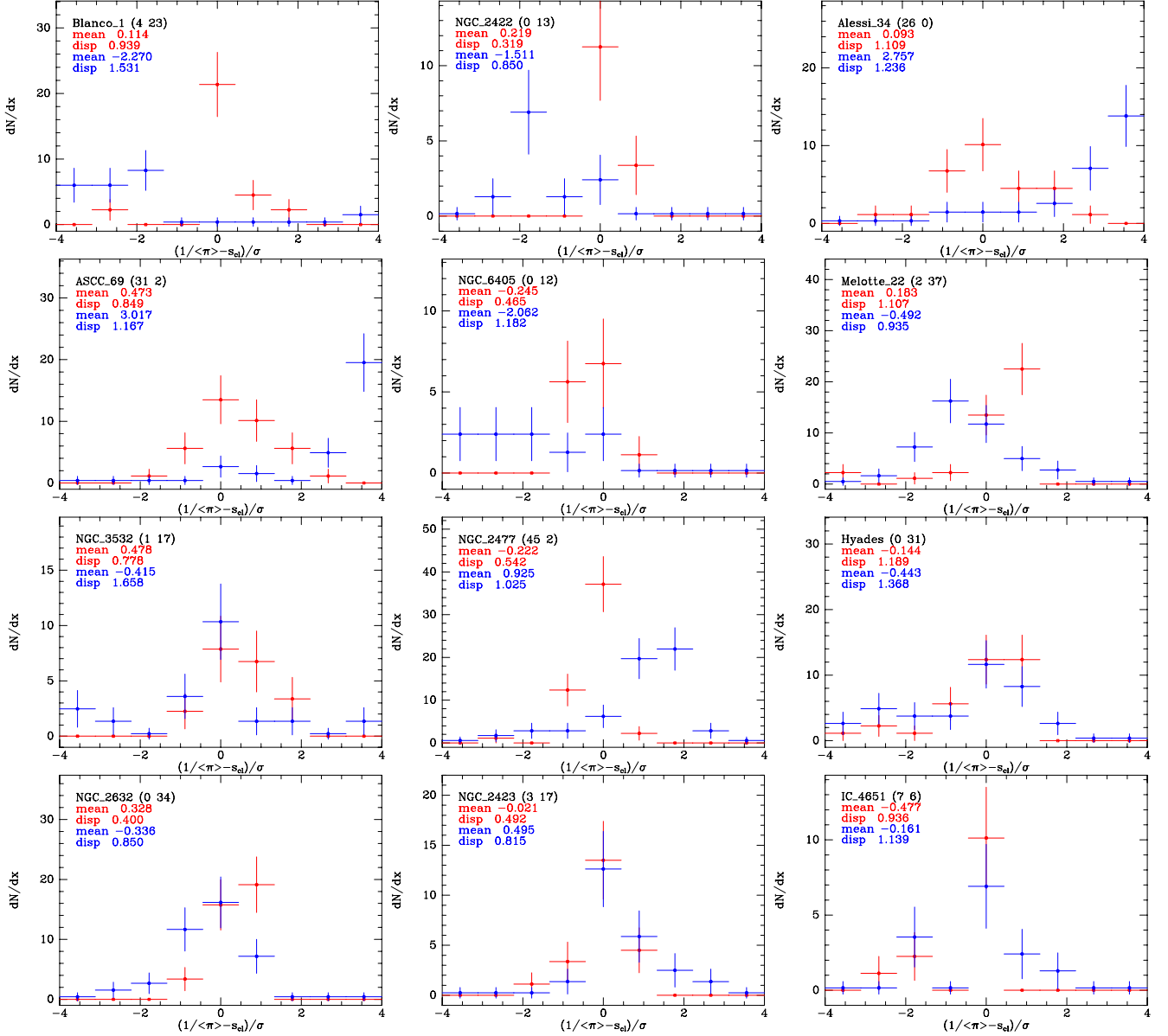
Figure 14. Histograms (in red) of the distances $1/\langle\varpi\rangle$ to stars in individual clusters (see Fig. 15 for NGC 2682). The blue points show results obtained when the prior on the age is a Gaussian in $\log\tau$ with dispersion 0.1 Gyr and centred on the literature value given in Table 10. The clusters are ordered from top left to bottom right by age. The numbers in parentheses after the cluster name give the number of giants and dwarfs contributing to the plot. The normalizing dispersion σ is the quadrature sum of the errors on the distances and the size of the cluster listed in Table 10. The blue points have been moved up slightly for clarity.

directions of anomalously low extinction, an effect that is captured when the extinction is estimated to be the fraction of the measured extinction to infinity that is expected to lie within distance s.

For hot dwarfs most values of $\widetilde{A}_V$ lie in (0.1, 0.25) [so $\widetilde{A}_J$ lies in (0.03, 0.07)], while a significant fraction of cool dwarfs have $\widetilde{A}_V < 0.1$ as we would expect given that some of these stars are quite close. The distribution of values of $\widetilde{A}_V$ for giants peaks around 0.2 but has a long tail extending out to ∼0.6 as we expect for stars that can be quite distant.

Fig. 19 shows histograms of the differences between our estimated extinctions $\widetilde{A}_V$ to stars in the complete sample and the value of the prior on extinction to the star's proposed location. The red, blue and black histograms are for stars that lie in three ranges of Galactic latitude b. The means of all the two highest latitude histograms are satisfyingly close to zero. The mean of the histogram

for $|b| < 20°$ is negative (-0.2σ), implying that the dust model slightly overestimates extinctions to low-latitude stars.

Fig. 20 shows the relationship between extinction and distance for hot dwarfs ($T_{\rm eff} > 5500$ K), cool dwarfs and giants ($\log g < 3.5$) in the full RAVE sample. In addition to showing the extent of the relation between distance and extinction, these plots show how the three classes of star are distributed in distance. The ridge line through the distribution of giants has a slope of $\simeq 0.19$ mag kpc^{-1}, while that through the distribution of cool dwarfs has a slope of $\simeq 0.78$ mag kpc^{-1}. For comparison, the traditional relation for paths near the mid-plane is $A_V \simeq 1.6\,s/$kpc (e.g. Binney & Merrifield 1998). Since most of our sight lines move away from the mid-plane, they naturally have lower values of extinction per unit length. Moreover, our samples are subject to the already-noted observational bias against stars' high extinctions, and this bias particularly
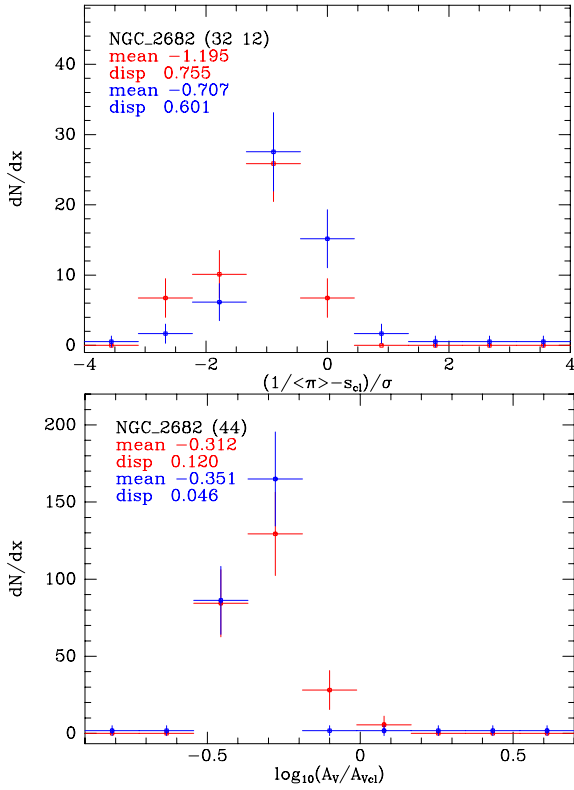
Figure 15. Upper panel: histogram of distances to stars in NGC 2682 (M87). The red points are obtained with the standard age prior and the blue points with prior that specifies the literature age of the cluster. Lower panel: histogram of ratios of extinctions of stars to the cluster's literature extinction. The red points denote the Bayesian extinctions and the blue points the priors from the Schlegel et al. map.

concentrates the giants at high latitudes, where extinction per unit distance is low.

The red points in Fig. 21 show for each cluster the distribution of $\log_{10}(\widetilde{A}_V/A_{V\mathrm{cl}})$, where $A_{V\mathrm{cl}}$ is 3.1 times the cluster's literature value of $E(B-V)$. The blue points show the corresponding distributions of the values obtained by replacing $\widetilde{A}_V$ by the prior extinction $A_{V\mathrm{prior}}$ at $1/\langle\varpi\rangle$. For all clusters the red and blue points have similar distributions, which suggests that the priors are reasonable. In light of this result, it is striking (a) how broad the distributions are, and (b) that in four clusters (Melotte 22, Hyades, NGC 2632 and NGC 2682) the literature extinction lies off one wing or the other of the distribution. These findings call into question the very concept of a cluster-wide characteristic extinction, and suggest that if one must choose a single characteristic extinction, the literature value may be a poor choice.

9 CONCLUSIONS

We have extended the Bayesian approach to distance determination of Burnett & Binney (2010) to allow for extinction and reddening and to deliver pdfs in distance modulus in addition to expectation values of three distance measures, distance s, distance modulus μ and parallax ϖ.

We have fitted each star's pdf in distance modulus with a sum of up to three Gaussians. A single Gaussian provides a good fit to about 45 per cent of the pdfs, two Gaussians provide a good fit to most of the remaining pdfs, so just 5 per cent of the pdfs require three Gaussians for a good fit. When these Gaussian decompositions are
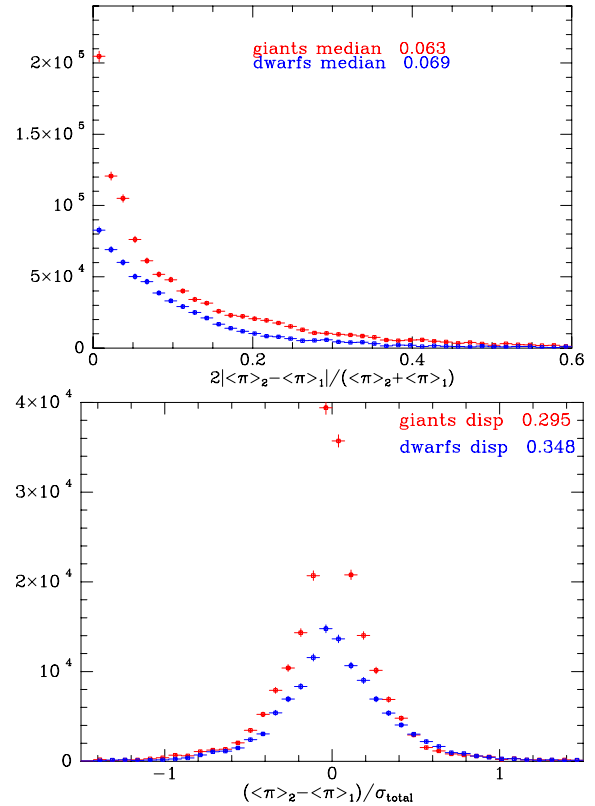

Figure 16. Discrepancies between different measurements of the distances of the same star.
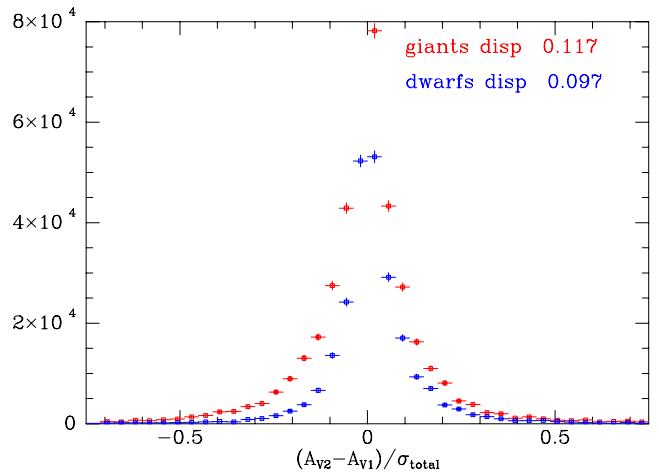

Figure 17. Discrepancies between different measurements of the extinctions to the same star.

used to make Hess diagrams by splitting each star's contribution to the density into one, two or three parts at the luminosity associated with the centre of each Gaussian component, the diagrams become significantly sharper as the main-sequence turnoff and the horizontal branch emerge clearly. This phenomenon indicates that multimodal pdfs are associated with stars that could be upper main-sequence stars or blue horizontal-branch stars, or could be lower main-sequence stars or subgiants.

For every class of star examined, we find that $\langle s\rangle > s_{\langle\mu\rangle} > 1/\langle\varpi\rangle$, a phenomenon that arises because these distance measures weight
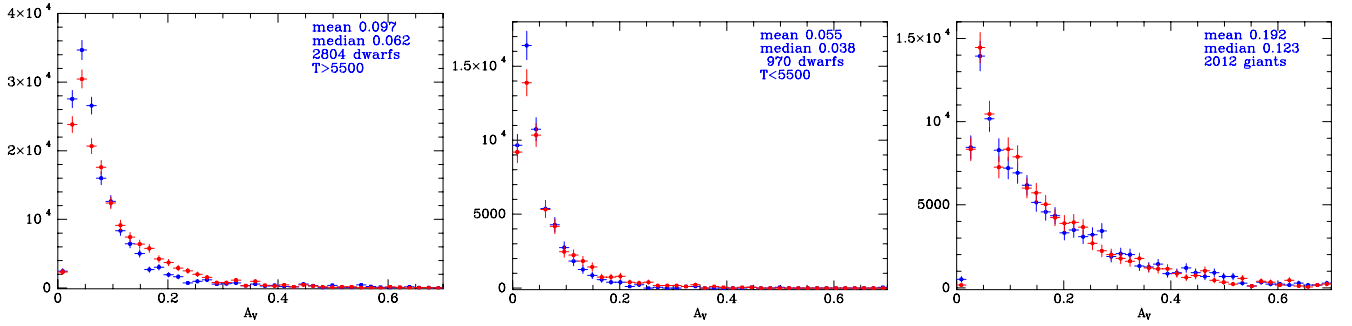
Figure 18. The blue points show the distributions of $\widetilde{A}_V$ for *Hipparcos* stars: hot dwarfs (left), cool dwarfs (centre) and giants (right). The red points show the distribution of the values of the prior extinction at the predicted locations of the stars.
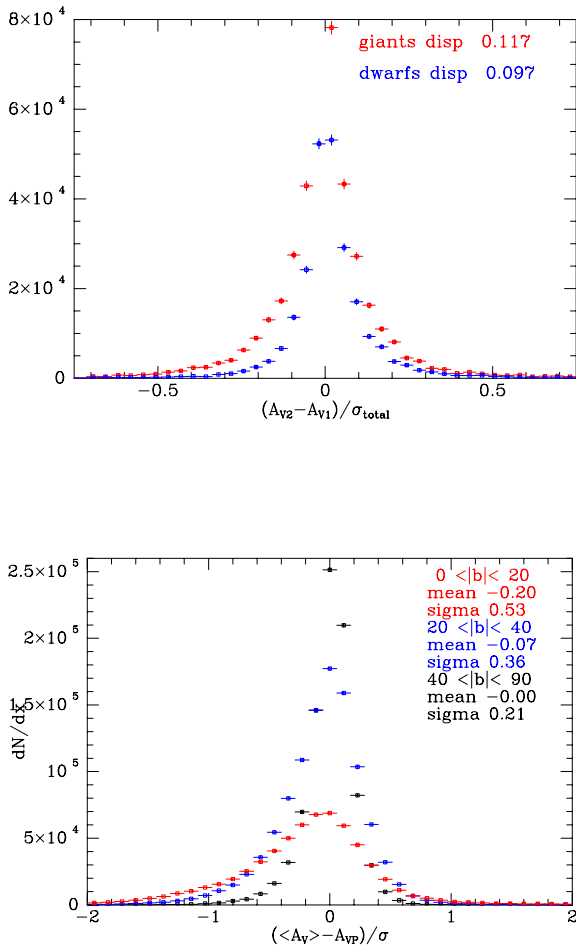

Figure 19. Histogram of the offsets between the estimated visual extinction $\widetilde{A}_V$ to stars in the complete RAVE sample and the extinction in the dust model used as a prior to the location $(l, b, 1/\langle \varpi \rangle)$.

differently the possibilities that a given star is far or near. The differences between these distance measures are least for hot dwarfs $T_{\rm eff} > 5500$ K and red clump stars, and greatest for very cool dwarfs ($T_{\rm eff} < 5200$ K) and high-gravity giants ($\log g > 2.4$) because hot dwarfs and red clump stars have quite narrow pdfs in distance while the dwarf/giant ambiguity causes cool dwarfs and high-gravity giants to have broad pdfs in distance.

The RAVE survey encompasses $\sim$5000 *Hipparcos* stars. Histograms of the difference between our values of $\langle \varpi \rangle$ and the

Hipparcos parallaxes normalized by the quadrature sum of our errors and the *Hipparcos* errors come close to the ideal of a unit Gaussian of zero mean in the cases of warm dwarfs ($T_{\rm eff} > 5500$ K) and giants ($\log g < 3.5$), so not only are our parallax estimates fairly reliable, but our error estimates are reasonable. The situation regarding the smaller sample of cool dwarfs is unsatisfactory. The majority of these stars require multi-Gaussian fits to their pdfs. When a *Hipparcos* parallax is available, it agrees within the errors with one of the Gaussians as one would wish. But the single Gaussians fitted to a minority of cool dwarfs yield parallaxes that are significantly larger than the *Hipparcos* parallaxes. Thus, our ability to determine distances to cool dwarfs is rather limited.

For giants our parallaxes are competitive with those of *Hipparcos*, but for cool dwarfs errors on *Hipparcos* parallaxes are smaller than the errors on ours by a factor of $\sim$3.

The good agreement between our parallaxes and the *Hipparcos* parallaxes suggests that $1/\langle \varpi \rangle$ is our most reliable estimator of distance, a conclusion we were able to confirm subsequently. Hence, we have concentrated on assessing the accuracy of the distance estimator $1/\langle \varpi \rangle$.

The *Hipparcos* stars in the RAVE survey reveal (Fig. 9) a tendency for our distances to the hottest dwarfs to be $\sim$15 per cent too small, while our distances to dwarfs with $T_{\rm eff} \sim 5000$ K are too large by about the same amount. Our distances to the coolest dwarfs are 20–30 per cent too small. The *Hipparcos* stars reveal that our distances to giants are too large by a factor that increases smoothly with decreasing $\log g$ from unity at $\log g = 3.5$ to $\sim$1.2 at the lowest gravities. This phenomenon may reflect our use of stellar parameters obtained under the assumption of LTE. However, it should be noted that Kordopatis et al. (2013) excise the cores of strong lines, where non-LTE effects will be most prominent.

The values of the kinematic corrections obtained by the method of SBA for all the giants and dwarfs in the RAVE sample confirm the results from the *Hipparcos* stars: $1/\langle \varpi \rangle$ is a more reliable distance estimator for cool stars than $\langle s \rangle$ and for dwarfs the ratio of $1/\langle \varpi \rangle$ to the true distance increases with decreasing $T_{\rm eff}$ except below $T_{\rm eff} \sim 4500$ K, where it drops abruptly. For dwarfs the SBA kinematic indicators agree moderately with each other and suggest that our distances tend to be too short by an amount that decreases with $T_{\rm eff}$ from $\gtrsim$20 per cent at the hot end to perfection at $T_{\rm eff} \simeq 5000$ K. The shape of the plot of the ratios of our distance to true distance agrees perfectly with the *Hipparcos* results, but there is a small vertical offset between the curves.

For giants $1/\langle \varpi \rangle$ has a tendency to be too large, by an amount that emerges equally from the *Hipparcos* results and the SBA kinematic corrector f_W. The ratio of our distance to the true distance increases with decreasing $\log g$ from $\sim$1.05 at the high-gravity end to $\sim$1.2
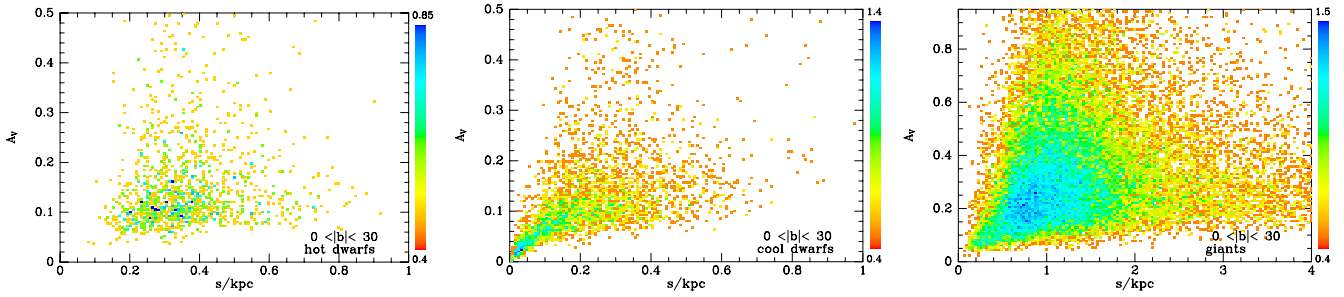
Figure 20. Density of stars in the distance versus extinction plane for hot dwarfs, cool dwarfs and giants in the range of Galactic latitudes $|b| < 30°$. The density scale is the same as in Fig. 12.
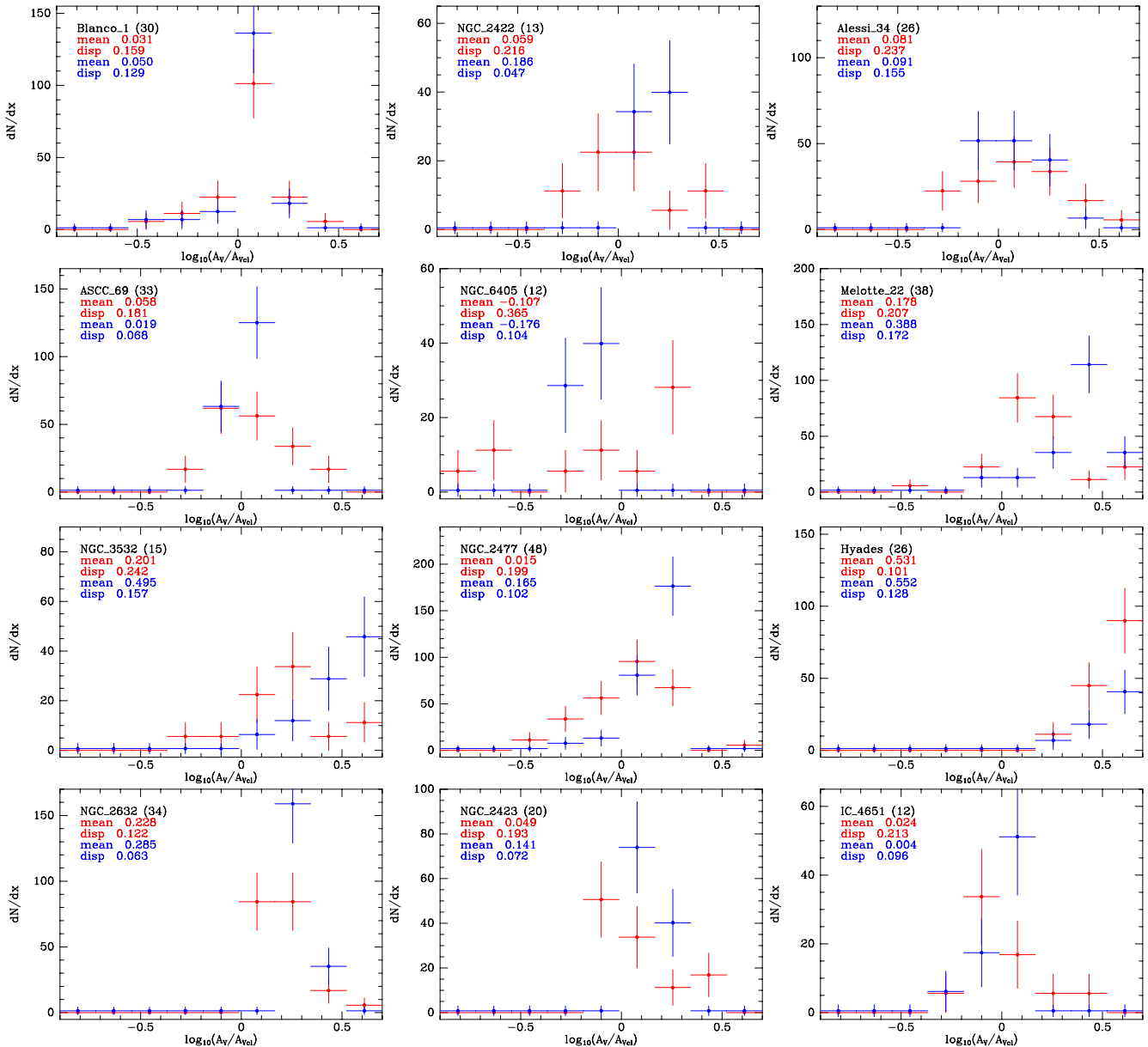

Figure 21. As Fig. 14 but showing in red the offsets of $\log_{10} \widetilde{A}_V$ from the cluster's literature value of $\log_{10} A_V$ (see Fig. 15 for NGC 2682). The blue points show the amounts by which the prior extinction at $1/\langle \varpi \rangle$ differs from the literature value. The blue points have been moved up slightly for clarity.

at the low-gravity end. Unfortunately, the *Hipparcos* results are of course confined to $s \lesssim 0.15\,\mathrm{kpc}$ and the SBA analysis proves sensitive to the upper limit on the distances of stars we use in the analysis. Moreover, for stars with $s \gtrsim 2\,\mathrm{kpc}$, the two SBA factors disagree with each other. Therefore, it is difficult to assess the accuracy of our distances to stars at $s > 2\,\mathrm{kpc}$, which tend to be luminous low-gravity giants. However, the indications are that we are overestimating these distances by $\gtrsim 20$ per cent.

We have identified red clump stars by cuts in the $(J - K, \log g)$ plane and found that a histogram of these stars' values of M_K is narrow and peaks ~ 0.1 mag fainter than the standard magnitude. The origin of this offset is unclear. If we accept the indications from both the *Hipparcos* stars and the SBA analysis that we systematically overestimate distances to giants, the offset is made significantly larger: 0.3 mag underluminous.

We have identified 364 RAVE stars in 15 open clusters. Our standard distances generally form a satisfyingly narrow distribution with the cluster's literature distance almost always within one standard deviation of the distribution's mean. There is a clear tendency for the giants in any cluster to be assigned distances that are larger than the distances assigned to the cluster's dwarfs. In the oldest clusters, IC 4651 and NGC 2682 (M67), the dwarf distances are only ~ 67 per cent of the cluster distance, but in the other clusters the dwarf distances appear about right.

The data barely constrain the ages of stars. Consequently, our standard distances are based on the assumption that stars are quite old, older than the ages of many of the clusters we have studied. Curiously, using a prior on ages that enforces the cluster's literature age produces a more satisfying histogram of distances only for clusters older than Melotte 22 (the Pleiades).

The data do contain sufficient information to place significant constraints on the extinctions of stars – we know this because the extinctions we first derived were systematically lower than the priors we then employed. This phenomenon led to improved priors, and our extinctions now scatter nearly randomly around the prior values. Since extinction varies discontinuously from one line of sight to the next on account of the fractal nature of the ISM, and we do not have a sample of stars with accurately determined extinctions, it is difficult to test the validity of our extinctions. Our results for clusters indicate that different stars in the same cluster generally have significantly different extinctions, and that the mean extinction of stars in a given cluster often differs significantly from the cluster's literature value.

The distances we derive from different spectra of the same star are entirely consistent with one another and imply that noise in the spectrum contributes less than half the uncertainty in the derived distance.

This work could and should be significantly improved in three ways. First, photometry in optical bands is now available for most of our stars from the APASS survey (Henden et al. 2012). Use of this photometry would sharpen constraints on some combination of A_V and T_{eff}. Secondly, the stellar models used here are now a few years old and should be updated and extended. Inclusion of α-enhanced stars with lower metallicities should improve accuracy for stars that are far from the plane. Moreover, we could now use models for which magnitudes in the 2MASS system have been directly computed rather than obtained by transformation of magnitudes in the Johnson–Cousins system. Thirdly, stellar parameters that include corrections for non-LTE effects as discussed by Ruchti et al. (2013) may yield improved distances, especially to luminous giants. Distances based on extended photometry and models will be made available on the RAVE website as soon as possible.

REFERENCES

Anotoja T., Helmi A., Bienaymé O., Bland-Hawthorn J., the RAVE collaboration, 2012, MNRAS, 425, L1
Arce H. G., Goodman A. A., 1999, ApJ, 512, L135
Aumer M., Binney J. J., 2009, MNRAS, 397, 1286
Bertelli G., Girardi L., Marigo P., Nasi E., 2008, A&A, 484, 815
Binney J., 2011, Pramana, 77, 39
Binney J., Merrifield M., 1998, Galactic Astronomy. Princeton Univ. Press, Princeton, NJ
Binney J. J., Gerhard O. E., Spergel D., 1997, MNRAS, 288, 365
Binney J. et al., 2013, MNRAS, preprint (arXiv:1309.4285)
Breddels M. A. et al., 2010, A&A, 511, 90
Burnett B, Binney J., 2010, MNRAS, 407, 339
Burnett B., Binney J., the RAVE collaboration, 2011, A&A, 532, 113 (B11)
Cannon R. D., 1970, MNRAS, 150, 111
Carollo D. et al., 2010, ApJ, 712, 692
Dehnen W., 1998, AJ, 115, 2384
Dias W. S., Alessi B. S., Moitinho A., Lepine J. R. D., 2002, A&A, 389, 871
Famay B., Jorissen A., Luri X., Mayor M., Udry S., Dejonghe H., Turon C., 2005, A&A, 430, 165
Gillessen S., Eisenhauer F., Trippe S., Alexander T., Genzel R., Martins F., Ott T., 2009, ApJ, 692, 1075
Haywood M., 2001, MNRAS, 325, 1365
Henden A. A., Levine S. E., Terrell D., Smith T. C., Welch D., 2012, J. Am. Assoc. Var. Star Obs., 40, 430
Jurić M. et al., 2008, ApJ, 673, 864
Koen C., Marang F., Kilkenny D., Jacobs C., 2007, MNRAS, 380, 1433
Kordopatis G. et al., 2013, AJ, 146, 134
Kroupa P., Tout C. A., Gilmore G., 1993, MNRAS, 262, 545
Laney C. D., Joner M. D., Pietrzynski G., 2012, MNRAS, 419, 1637
Perryman M. A. C. et al., 1998, A&A., 331, 81
Pietrzynski G., Gieren W., Udalski A., 2003, AJ, 125, 2494
Reddy B. E., 2009, in Cunha K., Spite M., Barbuy B., eds, Proc. IAU Symp. 265, Chemical Abundances in the Universe. Cambridge Univ. Press, Cambridge
Rieke G. H., Lebofsky R. M., 1985, ApJ, 288, 618
Röser S., Schilbach E., Schwan H., Kharchenko N. V., Piskunov A. E., Scholz R.-D., 2008, A&A, 488, 401
Ruchti G. R., Bergemann M., Serenelli A., Casagrande L., Lind K., 2013, MNRAS, 429, 126
Salaris M., 2013, in de Grijs R., ed., Proc. IAU Symp. 289, Advancing the Physics of Cosmic Distances. Cambridge Univ. Press, Cambridge
Schlegel D. J., Finkbeiner D. P., Davis M., 1998, ApJ, 500, 525
Schönrich R., Binney J., Asplund M., 2012a, MNRAS, 420, 1281 (SBA)

Schönrich R., Binney J., Dehnen W., 2012b, MNRAS, 403, 1829

Sharma S., Bland-Hawthorn J., Johnston K. V., Binney J., 2011, ApJ, 730, 3

Siebert A., Williams M. E. K., the RAVE collaboration, 2011, AJ, 141, 187

Steinmetz M. et al., 2006, AJ, 132, 1645

Strutskie M. F. et al., 2006, AJ, 131, 1163

van Leeuwen F., 2007, Hipparcos, the New Reduction of the Raw Data. Springer, Dordrecht

Williams M. E. K. et al., 2013, MNRAS, preprint (arXiv:1302.2468)

Yanny B. et al., 2009, AJ, 137, 4377

York D. G. et al., 2000, AJ, 120, 1579

Zwitter T. et al., 2008, AJ, 136, 421

Zwitter T. et al., 2010, A&A, 522, 54

This paper has been typeset from a TEX/LATEX file prepared by the author.